(Received 2 July 2025, Accepted 27 August 2025, Scheduled 8 September 2025)

Joint Beam Tracking Algorithm Research Based on RIS Selection

Chenwei Feng*, Zhenzhen Lin, Yawei Sun, Yangbin Huang, and Yinhua Wu

School of Opto-electronic and Communication Engineering, Xiamen University of Technology, Xiamen 361000, China

ABSTRACT: Reconfigurable Intelligent Surface (RIS), as one of the potential key technologies for 6G, can effectively solve the problem of millimeter-wave links being obstructed by constructing an intelligent and controllable wireless communication environment. In this paper, a joint beam tracking algorithm based on RIS selection is proposed for the scenario of multi-RIS-assisted millimeter-wave vehicle-to-infrastructure (V2I) communication. The aim is to select as few RISs as possible to aid communication while the performance of beam tracking can be maximized. Firstly, the beam tracking model jointly composed of line-of-sight paths and virtual line-of-sight paths constructed by multiple RISs is derived based on the multiple-input multiple-output model in a 3D road scene, and the beam tracking under this combined path is realized based on the Extended Kalman Filter (EKF) algorithm. Second, for the RIS-assisted millimeter-wave V2I scenario, a new metric to quantify the beam tracking performance is comprehensively designed based on the received signal-to-noise ratio, beam angle variation, and distance variation from the RIS to the vehicle. Finally, based on this metric, the joint beam tracking is realized by the RIS selection strategy and the EKF algorithm under the combined path. Simulation results show that the joint beam tracking algorithm based on RIS selection proposed in this paper has lower beam tracking error than the traditional signal-to-noise ratio based beam tracking algorithm.

1. INTRODUCTION

Vehicle wireless communication technology builds a "people - vehicle - road - cloud" collaborative Internet of vehicles (IoV) industrial ecosystem by realizing the information interaction between the vehicle and surrounding people, vehicles, infrastructure, and network, thus showing significant advantages in improving road traffic efficiency, reducing the rate of accidents, optimizing the scheduling of transportation resources, energy saving, emission reduction, etc. However, with the development of autonomous driving technology and smart cities, the demand for real-time interaction in vehicle-road cooperative autonomous driving systems is growing, and IoV technology is facing major challenges in realizing ultra-reliable and low-latency communication as well as high transmission rates [1–3].

Millimeter waves can support high data rates and low latency communications due to its abundant spectral resources [4]. At the same time, thanks to the physical characteristics of the shorter wavelength of millimeter waves, more antennas can be packaged in a smaller space, significantly improving the integration of antenna arrays [5]. By combining millimeter wave with Multiple-Input Multiple-Output (MIMO) technology, using beamforming technology can provide users with a highly directional narrow beam to achieve high-gain directional transmission, thus effectively compensating for the high path loss problem brought about by high-frequency communication [6–8]. Therefore, millimeter-wave MIMO is considered as a technology with development potential to meet the needs of the development of IoV. However, due to this high degree of directivity, even a small beam alignment deviation at the transmitter and receiver ends during communication can lead to a sharp drop in connectivity, causing communication to be interrupted. In addition, the effective formation of high-gain directional narrow beams requires accurate channel state information as a basis, which can be usually obtained through channel estimation, but this mostly applies to static environments. For rapidly changing channel environments, frequent channel estimation incurs significant training overhead. Therefore, a low-complexity beam tracking technique is urgently needed to achieve fast beam alignment at the receiver and transmitter ends and to ensure the stability of the communication link in highly dynamic IoV scenarios.

In addition, millimeter waves have poor rounding capabilities and rely heavily on the presence of Line of Sight (LoS) paths when communicating [9]. Packaging multiple antennas enables the formation of high-gain beams, but this also makes the problem of millimeter-wave signals' susceptibility to occlusion more significant. In high-density urban clusters, millimeter-wave beams can be easily blocked by high-rise buildings, trees, and large vehicles and thus fall into the signal blind zone, resulting in the failure of normal communication. Therefore, it is necessary to research the beam tracking technique to efficiently and accurately track millimeter-wave beams for stable data transmission and high-quality communication in the IoV scenario. Beam tracking plays an important role in achieving beam alignment and reducing training overhead. In addition, the 5G communication system uses ultra-high-frequency signals, which will result in the coverage radius of a single 5G base station being drastically shortened compared to the 4G system, and signal penetration will also be drastically weakened. As a result, more 5G base stations will be needed to cover the same large area to ensure connectivity and

* Corresponding author: Chenwei Feng (cwfeng@xmut.edu.cn).

stability of the communication link [10]. However, this would significantly increase the amount of demand for Base Stations (BS) or Road Side Units (RSUs) in a 5G network, so there is a need to cost-effectively re-engineer the communication system to enable millimeter-wave V2I communication at low cost.

RIS technology, with its programmable, low-cost, and low-power features, has been widely used in the field of wireless communication, which provides new ideas and methods to solve the above problems. RIS usually consists of a large number of electromagnetic units, each of which can be programmed to dynamically regulate the amplitude, phase, and frequency of the incident signal according to changes in the wireless channel [11–13]. The introduction of RIS significantly enhances the flexibility of the communication system and provides a brand new solution to break through the limitations of traditional wireless communication. In IoV system, when the LoS path of the Base Station User Equipment (BS-UE) is disconnected by obstacles, the Virtual Line of Sight (VLoS) transmission path constructed by RIS can be utilized to achieve reliable communication in the occluded area [14]. With the assistance of RIS, it effectively reduces the coverage blind spots of IoV in high-density urban clusters and improves network connectivity. When LoS paths are available, RIS can enhance the signal by providing additional transmission paths to extend the system coverage. In addition, the RIS utilizes a passive reflector unit architecture that passively reflects signals without the need to configure an active RF chain, thus avoiding the power consumption and signal processing delays inherent in traditional repeaters [15–17]. Therefore, the IoV system based on RIS assistance, on the one hand, can expand the signal coverage range while reducing the number of base stations or RSUs in the same area and lowering energy consumption and hardware costs. On the other hand, by adding reflection paths, a multipath transmission environment is created, providing more information such as beam angles and channel gains for beam tracking in millimeter-wave V2I communication, thereby effectively improving system performance.

Most previous studies on RIS-assisted wireless communication systems consider the case of a single RIS. However, relying only on a single RIS aid is difficult to meet the actual demand and cannot maximize the performance of the wireless communication system. Through multi-RIS deployment, on the one hand, multiple independent reflection paths can be artificially created to provide richer spatial information and improve communication quality. On the other hand, it can support more user communication and increase system capacity. Ref. [18] studied multi-RIS-assisted wireless communication systems and analyzed their error performance, achievable data rate, and path loss in both indoor and outdoor environments. Ref. [19] proposed a spatial orthogonality scheme based on the forced-zero technique for multi-RIS-assisted multi-user MIMO scenarios. The scheme can provide low-complexity and high-quality solutions to the weighted sum-rate maximization problem and transmit power minimization problem. Ref. [20] proposed an efficient cascaded channel estimation method based on compressed sensing theory as a solution to the problems of complex channel coupling and high overhead of multi-hop cascaded channel estimation in multi-RIS-assisted millimeter-wave communication systems.

At the same time, the use of multiple RISs to aid communication leads to an increase in the number of parameters in the system, requiring additional algorithms and strategies for signal processing and resource allocation. It increases the overall complexity and signaling overhead of the system. In addition, it is necessary to select RISs in terms of number and location in order to improve the energy efficiency of the system and to reduce the interference of reflected signals between RISs. Ref. [21] designed the RIS selection strategy by treating RIS selection problem as a stable matching problem for the multi-user multi-input single-output scenario assisted by multiple RISs. A two-stage user-RIS allocation algorithm is proposed to achieve stable user-RIS matching, thereby improving the system and rate. Ref. [22] chose instantaneous end-to-end Signal-to-Noise Ratio (SNR) highest RIS to assist the communication and interrupt probability, and the average and rate are studied. Ref. [23] studied the location-based optimal RIS selection strategy in RIS-assisted wireless networks for different path loss models and derived the distance distribution of optimal RIS node locations. Ref. [24] discussed the problem of RIS selection during uplink-transmission from vehicles to remote data centers. Vehicle selection provides RIS with the highest SNR corresponding to the first hop (from the vehicle to the RIS) as a relay, and deduces the traversal capacity and average symbol error probability, which are used as indicators for evaluating the performance of the scheme. Thus, it can be concluded that most of the current multi-RIS assisted communication systems use SNR as the index for RIS selection. SNR index is mostly used to evaluate cellular networks with circular coverage areas, and traditional multi-transport systems are also designed based on SNR. In the V2I network assisted by RIS, RSU and RIS are mostly deployed on both sides of the roads. Since most roads are relatively narrow and the distances between RSU, RIS and vehicles much shorter than the road length, the service coverage area under this network is approximately cut from a circle into a quadrilateral, which is different from the previous service areas [25–27]. Therefore, for the shape of the V2I service area assisted by RIS, merely selecting multiple RISs based on SNR is not comprehensive enough. Other dynamic factor changes brought about by vehicle mobility can also be considered to comprehensively design a new index for quantifying beam tracking performance.

In recent years, the combination of millimeter-wave communication and RIS has provided a new way to achieve high-speed, low-latency communication in the high-frequency band for V2X communication. However, existing research is mostly limited to single RIS scenarios and is unable to cope with complex urban scenarios involving multiple users, multiple paths, and multiple obstructions. Although multiple RIS deployments can provide more reflection paths, enhance link robustness, and improve beam tracking accuracy, they also increase complexity and overhead in terms of signal processing, resource scheduling, and interference management. Most existing RIS studies rely on SNR as an indicator to quantify beam tracking performance in RIS selection. However, in millimeter-wave V2I environments deployed along roads, due to the narrow cover-

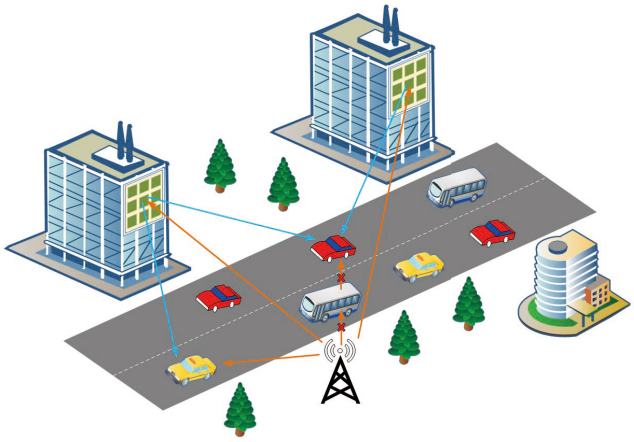

FIGURE 1. Scenario model.

age shape and high-speed movement characteristics of vehicles, a single SNR indicator cannot accurately reflect the dynamic changes in beam tracking performance. Therefore, it is necessary to design an RIS selection strategy that takes into account vehicle dynamics, coverage shape, and link stability in order to leverage the advantages of multiple RISs under conditions of low complexity and low cost, thereby improving beam tracking efficiency and communication stability.

Based on the above description, this paper proposes a joint beam tracking algorithm based on RIS selection for millimeter-wave V2I communication assisted by multiple RISs. This algorithm is designed for the V2I environment characterized by high-speed movement, frequent obstructions, and beam misalignment. This method selects an appropriate number and location of RIS by designing dynamic multi-factor fusion indicators, thereby retaining the coverage enhancement and multipath gain advantages of multiple RIS while significantly reducing training and signaling overhead, all at low complexity and low cost. This enhances beam tracking accuracy and link stability, providing an efficient and feasible technical solution for millimeter-wave communication in future high-dynamic V2X environments.

The main contributions of this paper are summarized as follows:

(1) In a 3D road scene, based on MIMO system model, a detailed derivation of the beam tracking model under a combined path was performed. This combined path includes the BS-UE LoS path and multiple VLoS paths constructed by multiple RISs to assist V2I communication. Based on EKF algorithm, the vehicle's motion state is predicted to achieve beam tracking under a combined path, thereby obtaining a joint beam tracking algorithm when multiple RISs participate in communication.

(2) A dynamic multi-factor fusion index was designed to comprehensively consider the received SNR, beam angle changes, and distance changes between the RIS and the vehicle, thereby more comprehensively quantifying beam tracking performance. This metric takes into account link quality, beam stability, and vehicle mobility, making it more suitable for the actual needs of highly dynamic road environments than single SNR assessment methods.

(3) Based on the designed dynamic multi-factor fusion index, this paper proposes a joint beam tracking algorithm based on RIS selection. When the vehicle is in moving state, the algorithm can dynamically select the optimal number and position of RIS to participate in communication, thereby maximizing beam tracking performance and further improving the stability of the communication link and overall system performance.

The rest of this paper is organized as follows. Section 2 describes the system model in detail. Section 3 introduces joint beam tracking based on RIS selection. Section 4 presents simulation results and analysis. Finally, Section 5 summarizes the entire paper.

2. SYSTEM MODEL

2.1. Scenario Model

Considering a unidirectional two-lane IoV scenario covered by a single RSU, where multiple RISs are deployed on the surface of a building on the side of the road in order to assist the RSUs in their communication, the studied scenario model is shown in Figure 1. Based on millimeter-wave MIMO, signal transmission and reception are carried out, that is, both RSU and vehicle users are equipped with multiple antennas. This article uses the passive reflection function of RIS in communication scenarios. The amplification of the reflected signal is not considered, that is, all passive RISs are deployed. This paper comprehensively considers the situation where not only the communication between RSU and vehicles can be conducted through LoS paths, but also the VLoS paths constructed by multiple RIS can be utilized simultaneously to assist in communication. When the target vehicle is blocked and disconnected from the LoS path due to the occlusion of other large vehicles on the road, the RSU maintains the connectivity of the communication link through the VLoS path.

2.2. Transmission Model

This paper focuses on the RIS-assisted downlink V2I communication process. A total of $\mathcal{I}$ RISs are deployed in the system. Since RSUs and RISs are deployed in a fixed manner, the locations of RSUs and RISs are accurately obtained in advance. In order to simplify the mathematical model, only the case of V2I communication for a single vehicle user is studied, and it is assumed that in the ideal case of no scattering points, there is only one communicable LoS path between the RIS and vehicle users, that there is no NLoS path due to scattering points, and that there are no signal reflections between the RISs that interfere with each other. Taking the position of the fixed deployed RSU as the origin, the direction of vehicle travel is defined as the x-axis; the direction perpendicular to it is defined as the y-axis; and the direction perpendicular to the road surface is defined as the z-axis, in order to establish a three-dimensional spatial coordinate system. The research model is shown in Figure 2. The RIS is deployed in the communication coverage area of the RSU to construct the VLoS path to reflect the communication beam. The number of antennas configured by the RSU and vehicle user are N_{BS} and N_{UE}, respectively, arranged in a Uniform Linear Array (ULA). Each RIS consists of $N_{\mathrm{RIS}} = N_{\mathrm{x}} \times N_{\mathrm{y}}$ re-

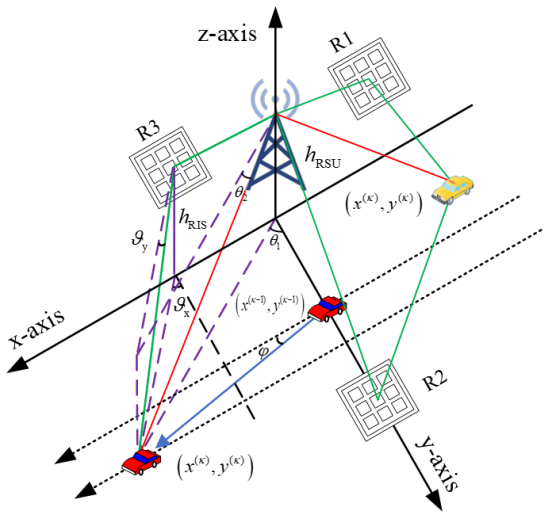

FIGURE 2. Research model.

flective units arranged in a UPA. Both antenna and unit spacing are set to $d = \lambda/2$, and λ is the signal wavelength. Due to the high path loss associated with millimeter-wave signals as they spread, the complexity, cost, and power consumption of the digital and hybrid beamforming hardware limit the application in millimeter-wave communications, despite their advantages in performance and flexibility. On the other hand, analog beamforming is widely used due to its low hardware cost and ease of realization, making it more suitable for millimeter-wave MIMO antenna arrays. Therefore, this paper focuses on the realization of directional beam transmission combining the analog beamforming architectures at both the transceiver and receiver ends.

The millimeter-wave MIMO channel at discrete time κ is next modeled based on extended Saleh-Valenzuela channel model without considering multi-cluster and multipath cases [28]. The directly connected channel $\mathbf{H}_{\mathrm{BU}}$ between BS-UE can be denoted as:

$$\mathbf{H}_{\mathrm{BU}}^{(\kappa)} = \beta_{\mathrm{BU}}^{(\kappa)} \mathbf{a}_{\mathrm{UE}}\left(\theta^{(\kappa)}\right) \mathbf{a}_{\mathrm{BS}}^{H}\left(\phi^{(\kappa)}\right) \tag{1}$$

where $\beta_{\mathrm{BU}}^{(\kappa)}$ is the channel gain coefficient. $\mathbf{a}_{\mathrm{BS}}(\phi^{(\kappa)})$ and $\mathbf{a}_{\mathrm{UE}}(\theta^{(\kappa)})$ denote the array response vectors at the BS side and UE side, respectively; θ is the Angle of Arrival (AOA) at the receiver side, and ϕ is the angle of departure (AOD) at the transmitter side. According to [29], as the receiver and transmitter communicate, the ULA direction of the RSU can be adjusted to be parallel to the vehicle traveling direction, when AoA and AoD are approximately equal. Therefore, in the rest of this paper, both AoA and AoD in the LoS path are denoted by ξ.

The channel $\mathbf{H}_{\mathrm{BR},i}$ from the BS to the ith RIS and the channel $\mathbf{H}_{\mathrm{RU},i}^{(\kappa)}$ from the ith RIS to the UE are denoted as:

$$\mathbf{H}_{\mathrm{BR},i} = \beta_{\mathrm{BR},i} \mathbf{a}_{\mathrm{RIS}}\left(\overline{\vartheta}_{\mathrm{x},i}, \overline{\vartheta}_{\mathrm{y},i}\right) \mathbf{a}_{\mathrm{BS}}^{\mathrm{H}}\left(\psi_{\mathrm{BS},i}\right) \tag{2}$$

$$\mathbf{H}_{\mathrm{RU},i}^{(\kappa)} = \beta_{\mathrm{RU},i}^{(\kappa)} \mathbf{a}_{\mathrm{UE}}\left(\psi_{\mathrm{UE},i}^{(\kappa)}\right) \mathbf{a}_{\mathrm{RIS}}^{\mathrm{H}}\left(\vartheta_{\mathrm{x},i}^{(\kappa)}, \vartheta_{\mathrm{y},i}^{(\kappa)}\right) \tag{3}$$

where $\beta_{\mathrm{BR},i}$ and $\beta_{\mathrm{RU},i}^{(\kappa)}$ are the channel gain coefficients of the two segmented subchannels, BS-RIS and RIS-UE. $\mathbf{a}_{\mathrm{RIS}}$ is the UPA response vector for RIS. $\psi_{\mathrm{BS},i}$ and $\psi_{\mathrm{UE},i}^{(\kappa)}$ denote the pointing direction of the beam at the BS and UE ends, respectively. $\overline{\vartheta}_{\mathrm{x},i}$ and $\overline{\vartheta}_{\mathrm{y},i}$ denote the azimuth and pitch angles of the beam in the ith RIS incidence direction, respectively. $\vartheta_{\mathrm{x},i}^{(\kappa)}$ and $\vartheta_{\mathrm{y},i}^{(\kappa)}$ denote the azimuth and pitch angles of the beam in the ith RIS reflection direction, respectively.

The gain coefficient $\beta_{\mathrm{BU}}^{(\kappa)}$ of the directly connected channel and the gain coefficients $\beta_{\mathrm{BR},i}$ and $\beta_{\mathrm{RU},i}^{(\kappa)}$ of the two segmented sub-channels can be respectively expressed as functions related to their corresponding link distances, as follows [29]:

$$\beta_{\mathrm{BU}}^{(\kappa)} = \tilde{\beta}(d_{\mathrm{BU}}^{(\kappa)})^{-1} e^{j\frac{2\pi}{\lambda} d_{\mathrm{BU}}^{(\kappa)}} = \tilde{\beta}(d_{\mathrm{BU}}^{(\kappa)})^{-1} e^{j\frac{2\pi f_c}{c} d_{\mathrm{BU}}^{(\kappa)}} \tag{4}$$

$$\beta_{\mathrm{BR},i} = \tilde{\beta} d_{\mathrm{BR},i}^{-1} e^{j\frac{2\pi}{\lambda} d_{\mathrm{BR},i}} = \tilde{\beta} d_{\mathrm{BR},i}^{-1} e^{j\frac{2\pi f_c}{c} d_{\mathrm{BR},i}} \tag{5}$$

$$\beta_{\mathrm{RU},i}^{(\kappa)} = \tilde{\beta}(d_{\mathrm{RU},i}^{(\kappa)})^{-1} e^{j\frac{2\pi}{\lambda} d_{\mathrm{RU},i}^{(\kappa)}} = \tilde{\beta}(d_{\mathrm{RU},i}^{(\kappa)})^{-1} e^{j\frac{2\pi f_c}{c} d_{\mathrm{RU},i}^{(\kappa)}} \tag{6}$$

where $d_{\mathrm{BU}}^{(\kappa)}$ is the distance between the BS and UE, $d_{\mathrm{BR},i}$ the distance between the BS and the ith RIS, $d_{\mathrm{RU},i}^{(\kappa)}$ the distance between the ith RIS and UE, and $\tilde{\beta}$ the channel power gain at a reference distance of 1 m. During the communication process, since the positions of BS and RIS are fixed, and the vehicle user is in a constantly moving state, then $d_{\mathrm{BR},i}$ is a fixed value, $d_{\mathrm{BU}}^{(\kappa)}$ and $d_{\mathrm{RU},i}^{(\kappa)}$ are time-varying values, that is, $\beta_{\mathrm{BR},i}$ is a fixed value, and β_{BU} and $\beta_{\mathrm{RU},i}^{(\kappa)}$ are time-varying values.

The ULA array response vectors at the BS side and UE side can be denoted as respectively:

$$\mathbf{a}_{\mathrm{BS}}(\alpha) = \frac{1}{\sqrt{N_{\mathrm{BS}}}}\left[1, e^{j\alpha}, \cdots, e^{j(N_{\mathrm{BS}}-1)\alpha}\right]^{T} \tag{7}$$

$$\mathbf{a}_{\mathrm{UE}}(\zeta) = \frac{1}{\sqrt{N_{\mathrm{UE}}}}\left[1, e^{j\zeta}, \cdots, e^{j(N_{\mathrm{UE}}-1)\zeta}\right]^{T} \tag{8}$$

where $\alpha \in \{\xi^{(\kappa)}, \psi_{\mathrm{BS},i}\}$, $\zeta \in \{\xi^{(\kappa)}, \psi_{\mathrm{UE},i}^{(\kappa)}\}$.

At the ith RIS, the UPA array response in the incident and reflected directions can be expressed as follows, respectively:

$$\mathbf{a}_{\mathrm{RIS}}\left(\overline{\vartheta}_{\mathrm{x},i}, \overline{\vartheta}_{\mathrm{y},i}\right) = \mathbf{a}_{\mathrm{x}}\left(\overline{\vartheta}_{\mathrm{x},i}\right) \otimes \mathbf{a}_{\mathrm{y}}\left(\overline{\vartheta}_{\mathrm{y},i}\right) \tag{9}$$

$$\mathbf{a}_{\mathrm{RIS}}\left(\vartheta_{\mathrm{x},i}^{(\kappa)}, \vartheta_{\mathrm{y},i}^{(\kappa)}\right) = \mathbf{a}_{\mathrm{x}}\left(\vartheta_{\mathrm{x},i}^{(\kappa)}\right) \otimes \mathbf{a}_{\mathrm{y}}\left(\vartheta_{\mathrm{y},i}^{(\kappa)}\right) \tag{10}$$

where $\otimes$ denotes the Kronecker product. The above two equations can be expressed in detail as:

$$\begin{aligned}&\mathbf{a}_{\mathrm{RIS}}\left(\overline{\vartheta}_{\mathrm{x},i}, \overline{\vartheta}_{\mathrm{y},i}\right)\\ &= \frac{1}{\sqrt{N_{\mathrm{RIS}}}}\left[1, e^{j\pi\cos\overline{\vartheta}_{\mathrm{x},i}}, \cdots, e^{j(N_{\mathrm{x}}-1)\pi\cos\overline{\vartheta}_{\mathrm{x},i}}\right]^{\mathrm{T}}\\ &\otimes\left[1, e^{j\pi\sin\overline{\vartheta}_{\mathrm{x},i}\cos\overline{\vartheta}_{\mathrm{y},i}}, \cdots, e^{j(N_{\mathrm{y}}-1)\pi\sin\overline{\vartheta}_{\mathrm{x},i}\cos\overline{\vartheta}_{\mathrm{y},i}}\right]^{\mathrm{T}}\end{aligned} \tag{11}$$

$$\mathbf{a}_{\text{RIS}}\left(\vartheta_{\text{x},i}^{(\kappa)},\vartheta_{\text{y},i}^{(\kappa)}\right) = \frac{1}{\sqrt{N_{\text{RIS}}}}\left[1,e^{j\pi\cos\vartheta_{\text{x},i}^{(\kappa)}},\cdots,e^{j(N_{\text{x}}-1)\pi\cos\vartheta_{\text{x},i}^{(\kappa)}}\right]^{\text{T}} \otimes\left[1,e^{j\pi\sin\vartheta_{\text{x},i}^{(\kappa)}\cos\vartheta_{\text{y},i}^{(\kappa)}},\cdots,e^{j(N_{\text{y}}-1)\pi\sin\vartheta_{\text{x},i}^{(\kappa)}\cos\vartheta_{\text{y},i}^{(\kappa)}}\right]^{\text{T}} \quad (12)$$

The cascading channel model from BS to UE via the ith RIS reflection can be expressed as follows:

$$\mathbf{H}_{\text{BRU},i}^{(\kappa)} = \mathbf{H}_{\text{RU},i}^{(\kappa)}\boldsymbol{\Theta}_{i}^{(\kappa)}\mathbf{H}_{\text{BR},i} \quad (13)$$

where the diagonal matrix $\boldsymbol{\Theta}_{i}^{(\kappa)} = \text{diag}(\tau_{i,1}\omega_{i,1}^{(\kappa)},\ \tau_{i,2}\omega_{i,2}^{(\kappa)},\ \ldots,\ \tau_{i,N_{\text{RIS}}}\omega_{i,N_{\text{RIS}}}^{(\kappa)})$ characterizes the amplitude and phase adjustment of the RIS to the incident electromagnetic wave. $\tau_{i,n} \in [0,1]$ denotes the reflection coefficient of the nth EMU of the ith RIS, and $\omega_{i,n}^{(\kappa)}$ is the phase shift parameter. It is assumed that the reflection coefficients of multiple RIS are all the same and are all set to 1, that is, $\tau_{i,n} = 1,\ i \in \{1,2,\cdots,\mathcal{I}\}$, $n \in \{1,2,\cdots,N_{\text{RIS}}\}$. Let $\boldsymbol{\omega}_{i}^{(\kappa)} = \left[\omega_{i,1}^{(\kappa)},\omega_{i,2}^{(\kappa)},\cdots,\omega_{i,N_{\text{RIS}}}^{(\kappa)}\right]$, then the diagonal matrix of the ith RIS at this time can be expressed as $\boldsymbol{\Theta}_{i}^{(\kappa)} = \text{diag}(\boldsymbol{\omega}_{i}^{(\kappa)})$.

The passive beamforming scheme given for RIS can be expressed as:

$$\boldsymbol{\omega}_{i}^{(\kappa)} = \mathbf{a}_{\text{RIS}}\left(\hat{\vartheta}_{\text{x},i}^{(\kappa-1)},\hat{\vartheta}_{\text{y},i}^{(\kappa-1)}\right) \odot \mathbf{a}_{\text{RIS}}^{\text{H}}\left(\overline{\vartheta}_{\text{x},i},\overline{\vartheta}_{\text{y},i}\right) \quad (14)$$

where $\odot$ denotes the Khatri-Rao product. $\hat{\vartheta}_{\text{x},i}^{(\kappa-1)}$ and $\hat{\vartheta}_{\text{y},i}^{(\kappa-1)}$ denote the estimates of azimuth and pitch angles based on the reflection angle of the ith RIS beam at the last time slot, respectively.

In summary, at discrete time κ, if the system selects $I \in [1,\mathcal{I}]$ RISs to assist the communication through the RIS selection strategy, the received signal at the vehicle is the superposition of the LoS path signal with multiple VLoS path signals, which can be expressed as:

$$\begin{aligned} r^{(\kappa)} &= \left(\sqrt{\rho_{\text{LoS}}^{(\kappa)}}\mathbf{w}_{\text{LoS}}^{H}\mathbf{H}_{\text{BU}}^{(\kappa)}\mathbf{f}_{\text{LoS}}^{(\kappa)} + \sum_{i=1}^{I}\sqrt{\rho_{\text{VLoS},i}^{(\kappa)}}\mathbf{w}_{\text{VLoS},i}^{H}\mathbf{H}_{\text{BRU},i}^{(\kappa)}\mathbf{f}_{\text{VLoS},i}\right)s + n^{(\kappa)} \\ &= \left(\sqrt{\rho_{\text{LoS}}^{(\kappa)}}\mathbf{w}_{\text{LoS}}^{H}\mathbf{H}_{\text{BU}}^{(\kappa)}\mathbf{f}_{\text{LoS}}^{(\kappa)} + \sum_{i=1}^{I}\sqrt{\rho_{\text{VLoS},i}^{(\kappa)}}\mathbf{w}_{\text{VLoS},i}^{H}\mathbf{H}_{\text{RU},i}^{(\kappa)}\boldsymbol{\Theta}_{i}^{(\kappa)}\mathbf{H}_{\text{BR},i}\mathbf{f}_{\text{VLoS},i}\right)s + n^{(\kappa)} \end{aligned} \quad (15)$$

where $\mathbf{w}$ is the simulated beam merging vector; $\mathbf{f}$ is the simulated beamforming vector satisfying $\|\mathbf{w}\|^2 = 1$ and $\|\mathbf{f}\|^2 = 1$; s is the normalized transmit signal; $n^{(\kappa)}$ is the additive Gaussian white noise at the UE end; $\rho^{(\kappa)}$ is the average SNR per antenna. Assuming unit antenna gain at the transmitter and receiver ends, this can be expressed through the Friesian transmission equation $\rho^{(\kappa)}$ as [25–27]:

$$\rho^{(\kappa)} = \frac{p}{\sigma_n^2}\left(\frac{\lambda}{4\pi d^{(\kappa)}}\right)^{n} \quad (16)$$

where p is the transmit power at the BS end, σ_n^2 the noise power, n the path loss index, λ the wavelength, and $d^{(\kappa)}$ the distance of the LoS path or VLoS path. This formula takes into account the influence of transmission distance on signal attenuation, that is, it considers the path loss problem of millimeter waves when they propagate in free space.

Let the beam pointing corresponding to the receiver and transmitter be $\overline{\xi}^{(\kappa)}$ when communicating using a direct-connected channel and the beam pointing corresponding to the receiver and transmitter are $\overline{\psi}_{\text{UE},i}^{(\kappa)}$ and $\overline{\psi}_{\text{BS},i}$, respectively, with communicating using a cascaded channel, then the beam merging vector $\mathbf{w}$ and beamforming vector $\mathbf{f}$ can be denoted as respectively:

$$\mathbf{w}\left(\overline{\zeta}\right) = \frac{1}{\sqrt{N_{\text{UE}}}}\left[1,e^{j\overline{\zeta}},\cdots,e^{j(N_{\text{UE}}-1)\overline{\zeta}}\right]^{T} \quad (17)$$

$$\mathbf{f}\left(\overline{\alpha}\right) = \frac{1}{\sqrt{N_{\text{BS}}}}\left[1,e^{j\overline{\alpha}},\cdots,e^{j(N_{\text{BS}}-1)\overline{\alpha}}\right]^{T} \quad (18)$$

where $\overline{\zeta} \in \{\overline{\xi}^{(\kappa)},\overline{\psi}_{\text{UE},i}^{(\kappa)}\}$, $\overline{\alpha} \in \{\overline{\xi}^{(\kappa)},\overline{\psi}_{\text{BS},i}\}$.

In Figure 2, the height of the RSU is h_{RSU}, and the deployment height of the ith RIS is $h_{\text{RIS},i}$. At discrete time κ, the vehicle user has coordinates $x^{(\kappa)}$ on the x-axis and $y^{(\kappa)}$ on the y-axis. The beam angles on the LoS path are decomposed into azimuth angles and elevation angles, which can be defined respectively as:

$$\sin\theta_1 = x\left(x^2+y^2\right)^{-\frac{1}{2}} \quad (19)$$

$$\cos\theta_2 = \left(x^2+y^2\right)^{\frac{1}{2}}\left(x^2+y^2+h_{\text{RSU}}^2\right)^{-\frac{1}{2}} \quad (20)$$

When the RSU communicates with the vehicle user over a direct channel, $\xi^{(\kappa)}$ can be expressed in terms of azimuth and pitch angles as:

$$\xi^{(\kappa)} = \pi\sin\theta_1\cos\theta_2 = \pi x\left(x^2+y^2+h_{\text{RSU}}^2\right)^{-\frac{1}{2}} \quad (21)$$

Similarly, the beam angles in the incident and reflected directions of the ith RIS are decomposed into azimuth and pitch angles, which can be defined as respectively:

$$\sin\overline{\vartheta}_{\text{x},i} = x_{\text{RIS},i}\left(x_{\text{RIS},i}^2+y_{\text{RIS},i}^2\right)^{-\frac{1}{2}} \quad (22)$$

$$\cos\overline{\vartheta}_{\text{y},i} = \left(x_{\text{RIS},i}^2+y_{\text{RIS},i}^2\right)^{\frac{1}{2}} \cdot\left(x_{\text{RIS},i}^2+y_{\text{RIS},i}^2+\left(h_{\text{RSU}}-h_{\text{RIS},i}\right)^2\right)^{-\frac{1}{2}} \quad (23)$$

$$\sin\vartheta_{\mathrm{x},i}^{(\kappa)} = (x - x_{\mathrm{RIS},i}) \cdot \left[(x - x_{\mathrm{RIS},i})^2 + (y - y_{\mathrm{RIS},i})^2\right]^{-\frac{1}{2}} \quad (24)$$

$$\cos\vartheta_{\mathrm{y},i}^{(x)} = \left[(x - x_{\mathrm{RIS},i})^2 + (y - y_{\mathrm{RIS},i})^2\right]^{\frac{1}{2}} \cdot \left[(x - x_{\mathrm{RIS},i})^2 + (y - y_{\mathrm{RIS},i})^2 + h_{\mathrm{RIS},i}^2\right]^{-\frac{1}{2}} \quad (25)$$

When the RSU communicates with the vehicle user over a cascaded channel, the beam angle $\psi_{\mathrm{BS},i}$ in the incident direction and the beam angle $\psi_{\mathrm{UE},i}^{(\kappa)}$ in the reflected direction of the ith RIS can be expressed by the corresponding azimuth and pitch angles, respectively, as:

$$\psi_{\mathrm{BS},i} = \pi \sin\overline{\vartheta}_{\mathrm{x},i} \cos\overline{\vartheta}_{\mathrm{y},i} = \pi x_{\mathrm{RIS},i}\left(x_{\mathrm{RIS},i}^2 + y_{\mathrm{RIS},i}^2 + (h_{\mathrm{RSU}} - h_{\mathrm{RIS},i})^2\right)^{-\frac{1}{2}} \quad (26)$$

$$\psi_{\mathrm{UE},i}^{(\kappa)} = \pi \sin\vartheta_{\mathrm{x},i}^{(\kappa)} \cos\vartheta_{\mathrm{y},i}^{(\kappa)} = \pi (x - x_{\mathrm{RIS},i}) \cdot \left[(x - x_{\mathrm{RIS},i})^2 + (y - y_{\mathrm{RIS},i})^2 + h_{\mathrm{RIS},i}^2\right]^{-\frac{1}{2}} \quad (27)$$

During the communication process, since the BS is deployed with the RIS fixed and the vehicle user in motion, for the same RIS, $\psi_{\mathrm{BS},i}$ is fixed, and $\xi^{(\kappa)}$ and $\psi_{\mathrm{UE},i}^{(\kappa)}$ are time-varying values. The transceivers all have estimated angles to which the pointing directions of the beams will be adjusted, so the pointing directions $\overline{\psi}_{\mathrm{UE},i}^{(\kappa)}$ and $\overline{\psi}_{\mathrm{BS},i}$ of the beam merger $\mathbf{w}$ and beamformer $\mathbf{f}$ are fixed values. Similarly, $\overline{\xi}^{(\kappa)}$ is also fixed. Therefore, the time variables in the channel are represented by $\beta_{\mathrm{BU}}^{(\kappa)}$, $\beta_{\mathrm{RU},i}^{(\kappa)}$, $\xi^{(\kappa)}$, and $\psi_{\mathrm{UE},i}^{(\kappa)}$ during the multi-RIS assisted V2I communication. Then, Eq. (15) can be rewritten as:

$$r^{(\kappa)} = \sqrt{\rho_{\mathrm{LoS}}^{(\kappa)}}\mathbf{w}_{\mathrm{LoS}}^H\left(\overline{\xi}^{(\kappa)}\right)\mathbf{H}_{\mathrm{BU}}\left(\beta_{\mathrm{BU}}^{(\kappa)}, \xi^{(\kappa)}\right)\mathbf{f}_{\mathrm{LoS}}\left(\overline{\xi}^{(\kappa)}\right)S + \sum_{i=1}^{I}\left[\sqrt{\rho_{\mathrm{VLoS},i}^{(\kappa)}}\mathbf{w}_{\mathrm{VLoS},i}^H\left(\overline{\psi}_{\mathrm{UE},j}^{(\kappa)}\right)\mathbf{H}_{\mathrm{RU},j}\left(\beta_{\mathrm{RU},i}^{(\kappa)}, \psi_{\mathrm{UE},j}^{(\kappa)}\right)\boldsymbol{\Theta}\left(\hat{\psi}_{\mathrm{UE},j}^{(\kappa)}\right)\mathbf{H}_{\mathrm{BR},j}\left(\psi_{\mathrm{BS},j}\right)\mathbf{f}_{\mathrm{VLoS},j}\left(\overline{\psi}_{\mathrm{BS},j}\right)s\right] + n^{(\kappa)} \quad (28)$$

3. JOINT BEAM TRACKING BASED ON RIS SELECTION

3.1. EKF Beam Tracking under Combined Paths

Assuming that the state information feedback has been performed after the uplink detection signal or that the RSU has obtained the state information of the vehicle at the initial moment through the existing initial channel access method, the focus is on the study about the RIS-assisted beam tracking after initializing the state information. Based on the vehicle position and speed to construct a state space model, the current vehicle user's state vector $\boldsymbol{\mu}^{(\kappa)}$, at discrete time κ, can be defined as:

$$\boldsymbol{\mu}^{(\kappa)} = \left[x^{(\kappa)}, y^{(\kappa)}, v^{(\kappa)}\right]^{\mathrm{T}} \quad (29)$$

where $x^{(\kappa)}$ and $y^{(\kappa)}$ are the coordinates of the vehicle user in the x and y axes, respectively, and $v^{(\kappa)}$ is the velocity. The system state equation can be expressed as:

$$\boldsymbol{\mu}^{(\kappa)} = \mathbf{A}\boldsymbol{\mu}^{(\kappa-1)} + \mathbf{W}^{(\kappa-1)} \quad (30)$$

where $\mathbf{w}^{(\kappa-1)} \sim \mathcal{CN}(0, \mathbf{Q}_\omega)$ is the error transfer vector at time $\kappa - 1$. According to the change model of vehicle motion, the state transition matrix can be expressed as:

$$\mathbf{A} = \begin{bmatrix} 1 & 0 & T_s\cos\varphi \\ 0 & 1 & T_s\sin\varphi \\ 0 & 0 & 1 \end{bmatrix} \quad (31)$$

The covariance matrix $\mathbf{Q}_\omega$ of the error transfer vector is denoted as:

$$\mathbf{Q}_\omega = \mathrm{diag}\left[T_s^2\sigma_\omega^2\cos^2\varphi, T_s^2\sigma_\omega^2\sin^2\varphi, \sigma_\omega^2\right] \quad (32)$$

where $\varphi \in [-\pi/2, \pi/2]$ is the vehicle steering angle, T_s the measurement period, and σ_ω^2 the variance of the speed error parameter. The speed error parameter is a hypothetical noise that is used to represent the change in vehicle speed [30].

Taking the received signal $r^{(\kappa)}$ as the system observation equation, Eq. (28) can be reexpressed as follows:

$$r^{(\kappa)} = \sqrt{\rho_{\mathrm{LoS}}^{(\kappa)}}\beta_{\mathrm{BU}}\left(d_{\mathrm{BU}}^{(\kappa)}\right)\mathbf{t}_{\mathrm{LoS}}\left(\xi^{(\kappa)}\right) + \sum_{i=1}^{I}\sqrt{\rho_{\mathrm{VLoS},i}^{(\kappa)}}\beta_{\mathrm{RU},i}\left(d_{\mathrm{RU},i}^{(\kappa)}\right)\mathbf{t}_{\mathrm{VLoS},i}\left(\psi_{\mathrm{UE},i}^{(\kappa)}\right) + n^{(\kappa)} \quad (33)$$

In order to facilitate the state prediction and correction process in the same domain, Eq. (33) is rewritten in the real number domain, namely:

$$\mathbf{r}^{(\kappa)} = \sqrt{\rho_{\mathrm{LoS}}^{(\kappa)}}\tilde{\beta}_{\mathrm{BU}}\left(d_{\mathrm{BU}}^{(\kappa)}\right)\tilde{\mathbf{t}}_{\mathrm{LoS}}\left(\xi^{(\kappa)}\right) + \sum_{i=1}^{I}\sqrt{\rho_{\mathrm{VLoS},i}^{(\kappa)}}\tilde{\beta}_{\mathrm{RU},i}\left(d_{\mathrm{RU},i}^{(\kappa)}\right)\tilde{\mathbf{t}}_{\mathrm{VLoS},i}\left(\psi_{\mathrm{UE},i}^{(\kappa)}\right) + \tilde{\mathbf{n}}^{(\kappa)} \quad (34)$$

where all variables contained in Eq. (34) are represented in the real field as follows:

$$\tilde{\mathbf{r}}^{(\kappa)} = \left[r^{(\kappa),\mathrm{re}}, r^{(\kappa),\mathrm{im}}\right]^{\mathrm{T}} \quad (35)$$

$$\tilde{\beta}_{\mathrm{BU}}^{(\kappa)} = \begin{bmatrix} \beta_{\mathrm{BU}}^{\mathrm{re}}\left(d_{\mathrm{BU}}^{(\kappa)}\right) & -\beta_{\mathrm{BU}}^{\mathrm{im}}\left(d_{\mathrm{BU}}^{(\kappa)}\right) \\ \beta_{\mathrm{BU}}^{\mathrm{im}}\left(d_{\mathrm{BU}}^{(\kappa)}\right) & \beta_{\mathrm{BU}}^{\mathrm{re}}\left(d_{\mathrm{BU}}^{(\kappa)}\right) \end{bmatrix} \quad (36)$$

$$\tilde{\beta}_{\mathrm{RU},i}^{(\kappa)} = \begin{bmatrix} \beta_{\mathrm{RU},i}^{\mathrm{re}}\left(d_{\mathrm{RU},i}^{(\kappa)}\right) & -\beta_{\mathrm{RU},i}^{\mathrm{im}}\left(d_{\mathrm{RU},i}^{(\kappa)}\right) \\ \beta_{\mathrm{RU},i}^{\mathrm{im}}\left(d_{\mathrm{RU},i}^{(\kappa)}\right) & \beta_{\mathrm{RU},i}^{\mathrm{re}}\left(d_{\mathrm{RU},i}^{(\kappa)}\right) \end{bmatrix} \quad (37)$$

$$\tilde{\mathbf{t}}_{\mathrm{LoS}}\left(\xi^{(\kappa)}\right) = \left[\mathbf{t}_{\mathrm{LoS}}^{\mathrm{re}}\left(\xi^{(\kappa)}\right), \mathbf{t}_{\mathrm{LoS}}^{\mathrm{im}}\left(\xi^{(\kappa)}\right)\right]^{\mathrm{T}} \quad (38)$$

$$\tilde{\mathbf{t}}_{\mathrm{VLoS},i}\left(\psi_{\mathrm{UE}}^{(\kappa)}\right) = \left[\mathbf{t}_{\mathrm{VLoS},i}^{\mathrm{re}}\left(\psi_{\mathrm{UE},i}^{(\kappa)}\right), \mathbf{t}_{\mathrm{VLoS},i}^{\mathrm{im}}\left(\psi_{\mathrm{UE},i}^{(\kappa)}\right)\right]^{\mathrm{T}} \quad (39)$$

$$\tilde{\mathbf{n}}^{(\kappa)} = \left[n^{(\kappa),\mathrm{re}}, n^{(\kappa),\mathrm{im}}\right]^{\mathrm{T}} \quad (40)$$

According to Eqs. (21) and (27), the function $\xi^{(\kappa)}$ of the beam direction on the LoS path at time κ and the function $\psi_{\mathrm{UE},i}^{(\kappa)}$ of the beam direction on the reflection path from the ith RIS to UE are defined as functions of the state vector, namely:

$$\xi^{(\kappa)} = \pi x\left(x^2+y^2+h_{\mathrm{RSU}}^2\right)^{-\frac{1}{2}} \doteq g_{\mathrm{LoS}}\left(\boldsymbol{\mu}^{(\kappa)}\right) \quad (41)$$

$$\begin{aligned}\psi_{\mathrm{UE},i}^{(\kappa)} &= \pi\left(x-x_{\mathrm{RIS},i}\right) \\ &\quad \cdot\left[\left(x-x_{\mathrm{RIS},i}\right)^2+\left(y-y_{\mathrm{RIS},i}\right)^2+h_{\mathrm{RIS},i}^2\right]^{-\frac{1}{2}} \\ &\doteq g_{\mathrm{VLoS},i}\left(\boldsymbol{\mu}^{(\kappa)}\right)\end{aligned} \quad (42)$$

Similarly, distances $d_{\mathrm{BU}}^{(\kappa)}$ and $d_{\mathrm{RU},i}^{(\kappa)}$ can be defined as functions of state vectors, namely:

$$d_{\mathrm{BU}}^{(\kappa)} = \left(x^2+y^2+h_{\mathrm{RSU}}^2\right)^{\frac{1}{2}} \doteq g_{\mathrm{BU}}\left(\boldsymbol{\mu}^{(\kappa)}\right) \quad (43)$$

$$\begin{aligned}d_{\mathrm{RU},i}^{(\kappa)} &= \left[\left(x-x_{\mathrm{RIS},i}\right)^2+\left(y-y_{\mathrm{RIS},i}\right)^2+h_{\mathrm{RIS},i}^2\right]^{\frac{1}{2}} \\ &\doteq g_{\mathrm{RU},i}\left(\boldsymbol{\mu}^{(\kappa)}\right)\end{aligned} \quad (44)$$

At this point, Eq. (34) can be rewritten as a function related to $g(\boldsymbol{\mu}^{(\kappa)})$:

$$\begin{aligned}\tilde{\mathbf{r}}^{(\kappa)} &= \sqrt{\rho_{\mathrm{LoS}}^{(\kappa)}}\,\tilde{\beta}_{\mathrm{BU}}\left(g_{\mathrm{BU}}\left(\boldsymbol{\mu}^{(\kappa)}\right)\right)\tilde{\mathbf{t}}_{\mathrm{LoS}}\left(g_{\mathrm{LoS}}\left(\boldsymbol{\mu}^{(\kappa)}\right)\right) \\ &\quad +\sum_{i=1}^{I}\sqrt{\rho_{\mathrm{VLoS},i}^{(\kappa)}}\,\tilde{\beta}_{\mathrm{RU},i}\left(g_{\mathrm{RU},i}\left(\boldsymbol{\mu}^{(\kappa)}\right)\right) \\ &\quad \tilde{\mathbf{t}}_{\mathrm{VLoS},i}\left(g_{\mathrm{VLoS},i}\left(\boldsymbol{\mu}^{(\kappa)}\right)\right)+\tilde{\mathbf{n}}^{(\kappa)} \\ &= \sqrt{\rho_{\mathrm{LoS}}^{(\kappa)}}\,\tilde{\mathbf{h}}_{\mathrm{LoS}}\left(\boldsymbol{\mu}^{(\kappa)}\right)+\sum_{i=1}^{I}\sqrt{\rho_{\mathrm{VLoS},i}^{(\kappa)}} \\ &\quad \tilde{\mathbf{h}}_{\mathrm{VLoS},i}\left(\boldsymbol{\mu}^{(\kappa)}\right)+\tilde{\mathbf{n}}^{(\kappa)}\end{aligned} \quad (45)$$

In summary, the channel vector can be expressed as:

$$\begin{aligned}\tilde{\mathbf{h}}_{\mathrm{LoS}}\left(\boldsymbol{\mu}^{(\kappa)}\right) &= \begin{bmatrix}\mathbf{h}_{\mathrm{LoS}}^{\mathrm{re}}\left(\boldsymbol{\mu}^{(\kappa)}\right) \\ \mathbf{h}_{\mathrm{LoS}}^{\mathrm{im}}\left(\boldsymbol{\mu}^{(\kappa)}\right)\end{bmatrix} \\ &= \begin{bmatrix}\beta_{\mathrm{BU}}^{(\kappa),\mathrm{re}}\mathbf{t}_{\mathrm{LoS}}^{(\kappa),\mathrm{re}}-\beta_{\mathrm{BU}}^{(\kappa),\mathrm{im}}\mathbf{t}_{\mathrm{LoS}}^{(\kappa),\mathrm{im}} \\ \beta_{\mathrm{BU}}^{(\kappa),\mathrm{im}}\mathbf{t}_{\mathrm{LoS}}^{(\kappa),\mathrm{re}}+\beta_{\mathrm{BU}}^{(\kappa),\mathrm{re}}\mathbf{t}_{\mathrm{LoS}}^{(\kappa),\mathrm{im}}\end{bmatrix}\end{aligned} \quad (46)$$

$$\begin{aligned}\tilde{\mathbf{h}}_{\mathrm{VLoS},i}\left(\boldsymbol{\mu}^{(\kappa)}\right) &= \begin{bmatrix}\mathbf{h}_{\mathrm{VLoS},i}^{\mathrm{re}}\left(\boldsymbol{\mu}^{(\kappa)}\right) \\ \mathbf{h}_{\mathrm{VLoS},i}^{\mathrm{im}}\left(\boldsymbol{\mu}^{(\kappa)}\right)\end{bmatrix} \\ &= \begin{bmatrix}\beta_{\mathrm{RU},i}^{(\kappa),\mathrm{re}}\mathbf{t}_{\mathrm{VLoS},i}^{(\kappa),\mathrm{re}}-\beta_{\mathrm{RU},i}^{(\kappa),\mathrm{im}}\mathbf{t}_{\mathrm{VLoS},i}^{(\kappa),\mathrm{im}} \\ \beta_{\mathrm{RU},i}^{(\kappa),\mathrm{im}}\mathbf{t}_{\mathrm{VLoS},i}^{(\kappa),\mathrm{re}}+\beta_{\mathrm{RU},i}^{(\kappa),\mathrm{re}}\mathbf{t}_{\mathrm{VLoS},i}^{(\kappa),\mathrm{im}}\end{bmatrix}\end{aligned} \quad (47)$$

The first-order Taylor series approximation of the channel vectors $\tilde{\mathbf{h}}_{\mathrm{LoS}}$ and $\tilde{\mathbf{h}}_{\mathrm{VLoS},i}$ obtained from the predicted state vector $\hat{\boldsymbol{\mu}}^{(\kappa|\kappa-1)}$ at the moment κ is:

$$\begin{aligned}\tilde{\mathbf{h}}_{\mathrm{LoS}}\left(\boldsymbol{\mu}^{(\kappa)}\right) &\simeq \tilde{\mathbf{h}}_{\mathrm{LoS}}\left(\hat{\boldsymbol{\mu}}^{(\kappa|\kappa-1)}\right) \\ &\quad +\tilde{\mathbf{G}}_{\mathrm{LoS}}^{(\kappa|\kappa-1)}\left(\boldsymbol{\mu}^{(\kappa)}-\hat{\boldsymbol{\mu}}^{(\kappa|\kappa-1)}\right)\end{aligned} \quad (48)$$

$$\begin{aligned}\tilde{\mathbf{h}}_{\mathrm{VLoS},i}\left(\boldsymbol{\mu}^{(\kappa)}\right) &\simeq \tilde{\mathbf{h}}_{\mathrm{VLoS},i}\left(\hat{\boldsymbol{\mu}}^{(\kappa|\kappa-1)}\right) \\ &\quad +\tilde{\mathbf{G}}_{\mathrm{VLoS},i}^{(\kappa|\kappa-1)}\left(\boldsymbol{\mu}^{(\kappa)}-\hat{\boldsymbol{\mu}}^{(\kappa|\kappa-1)}\right)\end{aligned} \quad (49)$$

Since the LoS path and each VLoS path are independent of each other, according to Eq. (45), Eq. (48), and Eq. (49), from the perspective of mathematical analysis, the independent received signals on each path can be approximately expressed as:

$$\begin{aligned}\tilde{\mathbf{r}}_{\mathrm{LoS}}^{(\kappa)} &\simeq \sqrt{\rho_{\mathrm{LoS}}^{(\kappa)}}\tilde{\mathbf{h}}_{\mathrm{LoS}}\left(\hat{\boldsymbol{\mu}}^{(\kappa|\kappa-1)}\right) \\ &+\sqrt{\rho_{\mathrm{LoS}}^{(\kappa)}}\tilde{\mathbf{G}}_{\mathrm{LoS}}^{(\kappa|\kappa-1)}\left(\boldsymbol{\mu}^{(\kappa)}-\hat{\boldsymbol{\mu}}^{(\kappa|\kappa-1)}\right)+\tilde{\mathbf{n}}_{\mathrm{LoS}}^{(\kappa)}\end{aligned} \quad (50)$$

$$\begin{aligned}\tilde{\mathbf{r}}_{\mathrm{VLoS},i}^{(\kappa)} &\simeq \sqrt{\rho_{\mathrm{VLoS},i}^{(\kappa)}}\tilde{\mathbf{h}}_{\mathrm{VLoS},i}\left(\hat{\boldsymbol{\mu}}^{(\kappa|\kappa-1)}\right) \\ &+\sqrt{\rho_{\mathrm{VLoS},i}^{(\kappa)}}\mathbf{G}_{\mathrm{VLoS},i}^{(\kappa|\kappa-1)}\left(\boldsymbol{\mu}^{(\kappa)}-\hat{\boldsymbol{\mu}}^{(\kappa|\kappa-1)}\right)+\tilde{\mathbf{n}}_{\mathrm{VLoS},i}^{(\kappa)}\end{aligned} \quad (51)$$

Assume that both $n_{\mathrm{LoS}}^{(\kappa)}$ and $n_{\mathrm{VLoS},i}^{(\kappa)}$ are normalized noise obeying a Gaussian distribution with mean 0 and variance 1. $\hat{\boldsymbol{\mu}}^{(\kappa|\kappa-1)}$ is an estimate based on the state vector $\boldsymbol{\mu}^{(\kappa)}$ at moment $\kappa-1$. $\tilde{\mathbf{G}}_{\mathrm{LOS}}^{(\kappa|\kappa-1)}$ and $\tilde{\mathbf{G}}_{\mathrm{VLOS},i}^{(\kappa|\kappa-1)}$ are Jacobi matrices, which can be expressed as:

$$\tilde{\mathbf{G}}_{\mathrm{LOS}}^{(\kappa|\kappa-1)} = \left[\dot{\mathbf{h}}_{\mathrm{LoS}}^{\mathrm{re}}\left(\hat{\boldsymbol{\mu}}^{(\kappa|\kappa-1)}\right), \dot{\mathbf{h}}_{\mathrm{LoS}}^{\mathrm{im}}\left(\hat{\boldsymbol{\mu}}^{(\kappa|\kappa-1)}\right)\right]^{T} \quad (52)$$

$$\tilde{\mathbf{G}}_{\mathrm{VLOS},i}^{(\kappa|\kappa-1)} = \left[\dot{\mathbf{h}}_{\mathrm{VLoS},i}^{\mathrm{re}}\left(\hat{\boldsymbol{\mu}}^{(\kappa|\kappa-1)}\right), \dot{\mathbf{h}}_{\mathrm{VLoS},i}^{\mathrm{im}}\left(\hat{\boldsymbol{\mu}}^{(\kappa|\kappa-1)}\right)\right]^{T} \quad (53)$$

the terms in the formula are respectively expressed as:

$$\dot{\mathbf{h}}_{\mathrm{LoS}}^{\mathrm{re}}\left(\hat{\boldsymbol{\mu}}^{(\kappa|\kappa-1)}\right) \doteq \beta_{\mathrm{BU}}^{\mathrm{re}}\left(g_{\mathrm{BU}}\left(\hat{\boldsymbol{\mu}}^{(\kappa|\kappa-1)}\right)\right)\dot{\mathbf{t}}_{\mathrm{LoS}}^{\mathrm{re}}\left(g_{\mathrm{LoS}}\left(\hat{\boldsymbol{\mu}}^{(\kappa|\kappa-1)}\right)\right)\dot{g}_{\mathrm{LoS}}\left(\hat{\boldsymbol{\mu}}^{(\kappa|\kappa-1)}\right)+\dot{\beta}_{\mathrm{BU}}^{\mathrm{re}}\left(g_{\mathrm{BU}}\left(\hat{\boldsymbol{\mu}}^{(\kappa|\kappa-1)}\right)\right)\dot{g}_{\mathrm{BU}}\left(\hat{\boldsymbol{\mu}}^{(\kappa|\kappa-1)}\right)$$
$$\mathbf{t}_{\mathrm{LoS}}^{\mathrm{re}}\left(g_{\mathrm{LoS}}\left(\hat{\boldsymbol{\mu}}^{(\kappa|\kappa-1)}\right)\right)-\beta_{\mathrm{BU}}^{\mathrm{im}}\left(g_{\mathrm{BU}}\left(\hat{\boldsymbol{\mu}}^{(\kappa|\kappa-1)}\right)\right)\dot{\mathbf{t}}_{\mathrm{LoS}}^{\mathrm{im}}\left(g_{\mathrm{LoS}}\left(\hat{\boldsymbol{\mu}}^{(\kappa|\kappa-1)}\right)\right)\dot{g}_{\mathrm{LoS}}\left(\hat{\boldsymbol{\mu}}^{(\kappa|\kappa-1)}\right)$$
$$-\dot{\beta}_{\mathrm{BU}}^{\mathrm{im}}\left(g_{\mathrm{BU}}\left(\hat{\boldsymbol{\mu}}^{(\kappa|\kappa-1)}\right)\right)\dot{g}_{\mathrm{BU}}\left(\hat{\boldsymbol{\mu}}^{(\kappa|\kappa-1)}\right)\mathbf{t}_{\mathrm{LoS}}^{\mathrm{im}}\left(g_{\mathrm{LoS}}\left(\hat{\boldsymbol{\mu}}^{(\kappa|\kappa-1)}\right)\right) \tag{54}$$

$$\dot{\mathbf{h}}_{\mathrm{LoS}}^{\mathrm{im}}\left(\hat{\boldsymbol{\mu}}^{(\kappa|\kappa-1)}\right) \doteq \beta_{\mathrm{BU}}^{\mathrm{im}}\left(g_{\mathrm{BU}}\left(\hat{\boldsymbol{\mu}}^{(\kappa|\kappa-1)}\right)\right)\dot{\mathbf{t}}_{\mathrm{LoS}}^{\mathrm{re}}\left(g_{\mathrm{LoS}}\left(\hat{\boldsymbol{\mu}}^{(\kappa|\kappa-1)}\right)\right)\dot{g}_{\mathrm{LoS}}\left(\hat{\boldsymbol{\mu}}^{(\kappa|\kappa-1)}\right)+\dot{\beta}_{\mathrm{BU}}^{\mathrm{im}}\left(g_{\mathrm{BU}}\left(\hat{\boldsymbol{\mu}}^{(\kappa|\kappa-1)}\right)\right)\dot{g}_{\mathrm{BU}}\left(\hat{\boldsymbol{\mu}}^{(\kappa|\kappa-1)}\right)$$
$$\mathbf{t}_{\mathrm{LoS}}^{\mathrm{re}}\left(g_{\mathrm{LoS}}\left(\hat{\boldsymbol{\mu}}^{(\kappa|\kappa-1)}\right)\right)+\beta_{\mathrm{BU}}^{\mathrm{re}}\left(g_{\mathrm{BU}}\left(\hat{\boldsymbol{\mu}}^{(\kappa|\kappa-1)}\right)\right)\dot{\mathbf{t}}_{\mathrm{LoS}}^{\mathrm{im}}\left(g_{\mathrm{LoS}}\left(\hat{\boldsymbol{\mu}}^{(\kappa|\kappa-1)}\right)\right)\dot{g}_{\mathrm{LoS}}\left(\hat{\boldsymbol{\mu}}^{(\kappa|\kappa-1)}\right)$$
$$+\dot{\beta}_{\mathrm{BU}}^{\mathrm{re}}\left(g_{\mathrm{BU}}\left(\hat{\boldsymbol{\mu}}^{(\kappa|\kappa-1)}\right)\right)\dot{g}_{\mathrm{BU}}\left(\hat{\boldsymbol{\mu}}^{(\kappa|\kappa-1)}\right)\mathbf{t}_{\mathrm{LoS}}^{\mathrm{im}}\left(g_{\mathrm{LoS}}\left(\hat{\boldsymbol{\mu}}^{(\kappa|\kappa-1)}\right)\right) \tag{55}$$

$$\dot{\mathbf{h}}_{\mathrm{VLoS},i}^{\mathrm{re}}\left(\hat{\boldsymbol{\mu}}^{(\kappa|\kappa-1)}\right) \doteq \beta_{\mathrm{RU},i}^{\mathrm{re}}\left(g_{\mathrm{RU},i}\left(\boldsymbol{\mu}^{(\kappa)}\right)\right)\dot{\mathbf{t}}_{\mathrm{VLoS},i}^{\mathrm{re}}\left(g_{\mathrm{VLoS},i}\left(\hat{\boldsymbol{\mu}}^{(\kappa|\kappa-1)}\right)\right)\dot{g}_{\mathrm{VLoS},i}\left(\hat{\boldsymbol{\mu}}^{(\kappa|\kappa-1)}\right)+\dot{\beta}_{\mathrm{RU},i}^{\mathrm{re}}\left(g_{\mathrm{RU},i}\left(\boldsymbol{\mu}^{(\kappa)}\right)\right)\dot{g}_{\mathrm{RU},i}\left(\boldsymbol{\mu}^{(\kappa)}\right)$$
$$\mathbf{t}_{\mathrm{VLoS},i}^{\mathrm{re}}\left(g_{\mathrm{VLoS},i}\left(\hat{\boldsymbol{\mu}}^{(\kappa|\kappa-1)}\right)\right)-\beta_{\mathrm{RU},i}^{\mathrm{im}}\left(g_{\mathrm{RU},i}\left(\boldsymbol{\mu}^{(\kappa)}\right)\right)\dot{\mathbf{t}}_{\mathrm{VLoS},i}^{\mathrm{im}}\left(g_{\mathrm{VLoS},i}\left(\hat{\boldsymbol{\mu}}^{(\kappa|\kappa-1)}\right)\right)\dot{g}_{\mathrm{VLoS},i}\left(\hat{\boldsymbol{\mu}}^{(\kappa|\kappa-1)}\right)$$
$$-\dot{\beta}_{\mathrm{RU},i}^{\mathrm{im}}\left(g_{\mathrm{RU},i}\left(\boldsymbol{\mu}^{(\kappa)}\right)\right)\dot{g}_{\mathrm{RU},i}\left(\boldsymbol{\mu}^{(\kappa)}\right)\mathbf{t}_{\mathrm{VLoS},i}^{\mathrm{im}}\left(g_{\mathrm{VLoS},i}\left(\hat{\boldsymbol{\mu}}^{(\kappa|\kappa-1)}\right)\right) \tag{56}$$

$$\dot{\mathbf{h}}_{\mathrm{VLoS},i}^{\mathrm{im}}\left(\hat{\boldsymbol{\mu}}^{(\kappa|\kappa-1)}\right) \doteq \beta_{\mathrm{RU},i}^{\mathrm{im}}\left(g_{\mathrm{RU},i}\left(\boldsymbol{\mu}^{(\kappa)}\right)\right)\dot{\mathbf{t}}_{\mathrm{VLoS},i}^{\mathrm{re}}\left(g_{\mathrm{VLoS},i}\left(\hat{\boldsymbol{\mu}}^{(\kappa|\kappa-1)}\right)\right)\dot{g}_{\mathrm{VLoS},i}\left(\hat{\boldsymbol{\mu}}^{(\kappa|\kappa-1)}\right)+\dot{\beta}_{\mathrm{RU},i}^{\mathrm{im}}\left(g_{\mathrm{RU},i}\left(\boldsymbol{\mu}^{(\kappa)}\right)\right)\dot{g}_{\mathrm{RU},i}\left(\boldsymbol{\mu}^{(\kappa)}\right)$$
$$\mathbf{t}_{\mathrm{VLoS},i}^{\mathrm{re}}\left(g_{\mathrm{VLoS},i}\left(\hat{\boldsymbol{\mu}}^{(\kappa|\kappa-1)}\right)\right)+\beta_{\mathrm{RU},i}^{\mathrm{re}}\left(g_{\mathrm{RU},i}\left(\boldsymbol{\mu}^{(\kappa)}\right)\right)\dot{\mathbf{t}}_{\mathrm{VLoS},i}^{\mathrm{im}}\left(g_{\mathrm{VLoS},i}\left(\hat{\boldsymbol{\mu}}^{(\kappa|\kappa-1)}\right)\right)\dot{g}_{\mathrm{VLoS},i}\left(\hat{\boldsymbol{\mu}}^{(\kappa|\kappa-1)}\right)$$
$$+\dot{\beta}_{\mathrm{RU},i}^{\mathrm{re}}\left(g_{\mathrm{RU},i}\left(\boldsymbol{\mu}^{(\kappa)}\right)\right)\dot{g}_{\mathrm{RU},i}\left(\boldsymbol{\mu}^{(\kappa)}\right)\mathbf{t}_{\mathrm{VLoS},i}^{\mathrm{im}}\left(g_{\mathrm{VLoS},i}\left(\hat{\boldsymbol{\mu}}^{(\kappa|\kappa-1)}\right)\right) \tag{57}$$

where the derivatives of the distance function and beam direction function are as follows:

$$\dot{g}_{\mathrm{BU}}\left(\hat{\boldsymbol{\mu}}^{(k|k-1)}\right) \doteq \frac{\left[\hat{x}^{(k|k-1)},\hat{\mathrm{y}}^{(k|k-1)},\cos\varphi\left(\hat{x}^{(k|k-1)}\right)T_s\right]}{\left(\left(\hat{x}^{(k|k-1)}\right)^2+\left(\hat{\mathrm{y}}^{(k|k-1)}\right)^2+h_{\mathrm{RSU}}^2\right)^{\frac{1}{2}}} \tag{58}$$

$$\dot{g}_{\mathrm{RU},i}\left(\boldsymbol{\mu}^{(\kappa)}\right) \doteq \frac{\left[\hat{x}^{(\kappa|\kappa-1)}-x_{\mathrm{RIS},i},\hat{\mathrm{y}}^{(\kappa|\kappa-1)}-y_{\mathrm{RIS},i},\cos\varphi\left(\hat{x}^{(\kappa|\kappa-1)}-x_{\mathrm{RIS},i}\right)T_s\right]}{\left[\left(\hat{x}^{(\kappa|\kappa-1)}-x_{\mathrm{RIS},i}\right)^2+\left(\hat{\mathrm{y}}^{(\kappa|\kappa-1)}-y_{\mathrm{RIS},i}\right)^2+h_{\mathrm{RIS},i}^2\right]^{\frac{1}{2}}} \tag{59}$$

$$\dot{g}_{\mathrm{LoS}}\left(\boldsymbol{\mu}^{(\kappa)}\right) \doteq \frac{\pi\left[\left(\hat{\mathrm{y}}^{(\kappa|\kappa-1)}\right)^2+h_{\mathrm{RSU}}^2,-\hat{x}^{(\kappa|\kappa-1)}\hat{\mathrm{y}}^{(\kappa|\kappa-1)},\cos\varphi\left(\left(\hat{\mathrm{y}}^{(\kappa|\kappa-1)}\right)^2+h_{\mathrm{RSU}}^2\right)T_s\right]}{\left(\left(\hat{x}^{(\kappa|\kappa-1)}\right)^2+\left(\hat{\mathrm{y}}^{(\kappa|\kappa-1)}\right)^2+h_{\mathrm{RSU}}^2\right)^{\frac{3}{2}}} \tag{60}$$

$$g_{\mathrm{VLoS},i}\left(\boldsymbol{\mu}^{(k|k-1)}\right) \doteq \frac{\pi\begin{bmatrix}\left(\hat{\mathrm{y}}^{(k|k-1)}-y_{\mathrm{RIS},i}\right)^2+h_{\mathrm{RIS},i}^2-\left(\hat{x}^{(k|k-1)}-x_{\mathrm{RIS},i}\right)\left(\hat{\mathrm{y}}^{(k|k-1)}-y_{\mathrm{RIS},i}\right)\\ \cos\varphi\left[\left(\hat{\mathrm{y}}^{(k|k-1)}-y_{\mathrm{RIS},i}\right)^2+h_{\mathrm{RIS},i}^2\right]T_s\end{bmatrix}^T}{\left[\left(\hat{x}^{(k|k-1)}-x_{\mathrm{RIS},i}\right)^2+\left(\hat{\mathrm{y}}^{(k|k-1)}-y_{\mathrm{RIS},i}\right)^2+h_{\mathrm{RIS},i}^2\right]^{\frac{3}{2}}} \tag{61}$$

The specific procedure of the EKF-based beam tracking algorithm for the communication system combining LoS paths and multiple RIS-assisted VLoS paths are as follows:

(1) State forecast update

$$\hat{\boldsymbol{\mu}}^{(\kappa|\kappa-1)}=\mathbf{A}\hat{\boldsymbol{\mu}}^{(\kappa-1|\kappa-1)} \tag{62}$$

(2) Calculate a priori covariance matrix

$$\mathbf{P}^{(\kappa|\kappa-1)}=\mathbf{A}\mathbf{P}^{(\kappa-1|\kappa-1)}\mathbf{A}^T+\mathbf{Q}_{\omega} \tag{63}$$

(3) Kalman gain matrix update

$$\mathbf{K}^{(\kappa)} = \mathbf{P}^{(\kappa|\kappa-1)}\left(\left(\boldsymbol{\rho}^{(\kappa)}\otimes\mathbf{I}_2\right)\tilde{\mathbf{G}}^{(\kappa|\kappa-1)}\right)^T$$
$$\times\left(\left(\boldsymbol{\rho}^{(\kappa)}\otimes\mathbf{I}_2\right)\tilde{\mathbf{G}}^{(\kappa|\kappa-1)}\mathbf{P}^{(\kappa|\kappa-1)}\right.$$
$$\left.\left(\left(\boldsymbol{\rho}^{(\kappa)}\otimes\mathbf{I}_2\right)\tilde{\mathbf{G}}^{(\kappa|\kappa-1)}\right)^T+\frac{\mathbf{I}_{2|I+1|}}{2}\right)^{-1} \tag{64}$$

where $\boldsymbol{\rho}^{(\kappa)} = \mathrm{diag}\left(\left[\sqrt{\rho_{\mathrm{LoS}}^{(\kappa)}},\sqrt{\rho_{\mathrm{VLoS},1}^{(\kappa)}},\cdots,\sqrt{\rho_{\mathrm{VLoS},I}^{(\kappa)}}\right]\right)$, $\mathbf{K}^{(\kappa)}$ are the Kalman gain matrices of the KF process, $\tilde{\mathbf{G}}^{(\kappa|\kappa-1)} = \left[\tilde{\mathbf{G}}_{\mathrm{LoS}}^{(\kappa|\kappa-1)},\tilde{\mathbf{G}}_{\mathrm{VLoS},1}^{(\kappa|\kappa-1)},\cdots,\tilde{\mathbf{G}}_{\mathrm{VLoS},I}^{(\kappa|\kappa-1)}\right]^T$, and $\mathbf{I}$ represent the unit matrices.

(4) Update the a posteriori value of the system state estimate

$$\hat{\boldsymbol{\mu}}^{(\kappa|\kappa)} = \hat{\boldsymbol{\mu}}^{(\kappa|\kappa-1)} + \mathbf{K}^{(\kappa)}\left(\tilde{\mathbf{s}}^{(\kappa)} - \left(\boldsymbol{\rho}^{(\kappa)} \otimes \mathbf{I}_2\right) \tilde{\mathbf{h}}\left(\hat{\boldsymbol{\mu}}^{(\kappa|\kappa-1)}\right)\right) \tag{65}$$

where $\tilde{\mathbf{h}}(\hat{\boldsymbol{\mu}}^{(\kappa|\kappa-1)}) = [(\tilde{\mathbf{h}}_{\text{LoS}}(\hat{\boldsymbol{\mu}}^{(\kappa|\kappa-1)}))^T, (\tilde{\mathbf{h}}_{\text{VLoS},1}(\hat{\boldsymbol{\mu}}^{(\kappa|\kappa-1)}))^T, \ldots, (\tilde{\mathbf{h}}_{\text{VLoS},I}\left(\hat{\boldsymbol{\mu}}^{(\kappa|\kappa-1)}\right))^T]^T$ is the channel vector, and $\tilde{\mathbf{s}}^{(\kappa)} = [(\tilde{\mathbf{r}}_{\text{LoS}}^{(\kappa)})^T, (\tilde{\mathbf{r}}_{\text{VLoS},1}^{(\kappa)})^T, \ldots, (\tilde{\mathbf{r}}_{\text{VLoS},I}^{(\kappa)})^T]^T$ is the received signal expression.

(5) Update the a posteriori covariance matrix

$$\mathbf{P}^{(\kappa|\kappa)} = \left(\mathbf{I}_3 - \mathbf{K}^{(\kappa)}\left(\boldsymbol{\rho}^{(\kappa)} \otimes \mathbf{I}_2\right)\tilde{\mathbf{G}}^{(\kappa|\kappa-1)}\right)\mathbf{P}^{(\kappa|\kappa-1)} \tag{66}$$

The above is done for one round of iteration. The required system state estimates for each moment, including the vehicle user's position and velocity information, can be obtained by continuous iteration.

3.2. Indicator Design Based on Dynamic Multifactor Fusion

In vehicular communications, SNR is usually used as a metric to quantify the beam tracking performance for RIS selection. In this paper, distinguishing from the traditional RIS selection metrics, a new metric for quantifying beam tracking performance is redesigned based on RIS-assisted V2I scenarios as a way to provide better beam tracking performance.

Next, the quantitative metrics are mainly designed for the scenario where the LoS path is obscured and switches to the VLoS path constructed by multiple RISs to maintain communication. In this paper, the elements affecting the beam tracking performance are analyzed by starting with the state transfer error $\mathbf{e}^{(\kappa|\kappa-1)} \doteq \boldsymbol{\mu}^{(\kappa)} - \hat{\boldsymbol{\mu}}^{(\kappa|\kappa-1)}$ in the EKF state update process. According to Eq. (65), the observed values are compared with the estimated values, that is

$$\begin{aligned}\Delta^{(\kappa)} &= \tilde{\mathbf{r}}_{\text{VLoS},i}^{(\kappa)} - \sqrt{\rho_{\text{VLoS},i}^{(\kappa)}}\tilde{\beta}_{\text{RU},i}^{(\kappa)}\tilde{\mathbf{h}}_{\text{VLoS},i}\left(g_{\text{VLoS},i}\left(\hat{\boldsymbol{\mu}}^{(\kappa|\kappa-1)}\right)\right) \\ &\simeq \sqrt{\rho_{\text{VLoS},i}^{(\kappa)}}\tilde{\beta}_{\text{RU},i}^{(\kappa)}\mathbf{G}_{\text{VLoS},i}^{(\kappa|\kappa-1)}\mathbf{e}^{(\kappa|\kappa-1)} + \tilde{\mathbf{n}}_{\text{VLoS},i}^{(\kappa)}\end{aligned} \tag{67}$$

From the above equation, it can be seen that there is a high correlation between the Jacobi matrix $\mathbf{G}_{\text{VLoS},i}^{(\kappa|\kappa-1)}$ and the state transfer error. As the vehicle user moves, $\mathbf{G}_{\text{VLoS},i}^{(\kappa|\kappa-1)}$ as an influence factor affects the prediction accuracy of the EKF algorithm and the performance of beam tracking at all times by correcting the state transfer error. According to Eq. (53), Eq. (56), and Eq. (57), $\mathbf{G}_{\text{VLoS},i}^{(\kappa|\kappa-1)}$ contains the degree of variation of the beam angle as well as the distance between the RIS and the vehicle with respect to the state information. According to the positions of BS, RIS and the vehicle, it can be analyzed from Eq. (27) that even if the distance traveled by the vehicle is the same, the change of the beam angle may also vary greatly. As the angle change due to vehicle motion becomes larger, the state update process will become noise independent. Therefore, in the millimeter-wave beam tracking process, not only can the received SNR be used to evaluate the strength of the transmitted signal, but also the beam angle and the degree of change in the distance from the RIS to the vehicle can be jointly used as a correction component to improve the accuracy of beam tracking, and a new index to quantify the performance of beam tracking can be obtained by fusing the multiple dynamic factors mentioned above.

The design process regarding the quantitative metrics is as follows. First, the performance of beam tracking is partially measured by the received SNR. The received SNR obtained by the vehicle users through the ith VLoS path is:

$$\varpi_i^{(\kappa)} = \frac{p\lambda^n\left(\mathbf{w}_{\text{VLoS},i}^H\mathbf{H}_{\text{BRU},i}^{(\kappa)}\mathbf{f}_{\text{VLoS},i}\right)^2}{\sigma_n^2\left(4\pi d_{\text{VLoS},i}^{(\kappa)}\right)^n} \tag{68}$$

It is known that the vehicle has a deflection in its driving direction during operation. However, since the main forward direction of the vehicle is the x-axis, the movement amplitude on the y-axis within each time slot is relatively small. Therefore, the beam angle and the changes in the distance between RIS and the vehicle on the y-axis are not discussed at this time. $T_s \ll 1$, thus we obtain:

$$\dot{g}_{\text{VLoS},i}^{(\kappa|\kappa-1)} \simeq \frac{\pi\left(\left(\hat{y}^{(\kappa|\kappa-1)} - y_{\text{RIS},i}\right)^2 + h_{\text{RIS},i}^2\right)[1,0,0]}{\left[\left(\hat{x}^{(\kappa|\kappa-1)} - x_{\text{RIS},i}\right)^2 + \left(\hat{y}^{(\kappa|\kappa-1)} - y_{\text{RIS},i}\right)^2 + h_{\text{RIS},i}^2\right]^{\frac{3}{2}}} \tag{69}$$

$$\dot{g}_{\text{RU},i}^{(\kappa|\kappa-1)} \simeq \frac{\left(\hat{x}^{(\kappa|\kappa-1)} - x_{\text{RIS},i}\right)[1,0,0]}{\left[\left(\hat{x}^{(\kappa|\kappa-1)} - x_{\text{RIS},i}\right)^2 + \left(\hat{y}^{(\kappa|\kappa-1)} - y_{\text{RIS},i}\right)^2 + h_{\text{RIS},i}^2\right]^{\frac{1}{2}}} \tag{70}$$

Secondly, the beam tracking performance is jointly measured in another part by the variation of the beam angle and the variation of the distance between the RIS and the vehicle, namely:

$$\zeta_i^{(\kappa|\kappa-1)} = \left[\left(\dot{g}_{\text{VLoS},i}^{(\kappa|\kappa-1)}\right)_{1,1} \cdot \left(\dot{g}_{\text{RU},i}^{(\kappa|\kappa-1)}\right)_{1,1}\right]^2 = \frac{\pi^2\left(\left(\left(\hat{y}^{(\kappa|\kappa-1)} - y_{\text{RIS},i}\right)^2 + h_{\text{RIS},i}^2\right)\left(\hat{x}^{(\kappa|\kappa-1)} - x_{\text{RIS},i}\right)\right)^2}{\left[\left(\hat{x}^{(\kappa|\kappa-1)} - x_{\text{RIS},i}\right)^2 + \left(\hat{y}^{(\kappa|\kappa-1)} - y_{\text{RIS},i}\right)^2 + h_{\text{RIS},i}^2\right]^4} \tag{71}$$

where $(\dot{g}_{\text{VLoS},i}^{(\kappa|\kappa-1)})_{1,1}$ and $(\dot{g}_{\text{RU},i})_{1,1}$ denote item $(1,1)$ of $\dot{g}_{\text{VLoS},i}^{(\kappa|\kappa-1)}$ and $\dot{g}_{\text{RU},i}$, respectively.

Finally, $\varsigma_i^{(\kappa|\kappa-1)}$ is fused with the received SNR as a correction component, both to correct for state transfer errors and to reflect the degree of influence with the noise component. According to Eq. (68) and Eq. (71), in the RIS assisted millimeter-wave V2I scenario, a new index for quantifying beam tracking performance was obtained, namely

$$\gamma_i^{(\kappa|\kappa-1)} = \varpi_i^{(\kappa)} \cdot \zeta_i^{(\kappa|\kappa-1)} = \frac{p\lambda^n\pi^2\left(\mathbf{w}_{\mathrm{VLoS},i}^H\mathbf{H}_{\mathrm{BRU},i}^{(\kappa)}\mathbf{f}_{\mathrm{VLoS},i}\right)^2\left(\left(\left(\hat{y}^{(\kappa|\kappa-1)}-y_{\mathrm{RIS},i}\right)^2+h_{\mathrm{RIS},i}^2\right)\left(\hat{x}^{(\kappa|\kappa-1)}-x_{\mathrm{RIS},i}\right)\right)^2}{\sigma_n^2\left(4\pi d_{\mathrm{VLoS},i}^{(\kappa)}\right)^n\left[\left(\hat{x}^{(\kappa|\kappa-1)}-x_{\mathrm{RIS},i}\right)^2+\left(\hat{y}^{(\kappa|\kappa-1)}-y_{\mathrm{RIS},i}\right)^2+h_{\mathrm{RIS},i}^2\right]^4} \tag{72}$$

3.3. EKF Joint Beam Tracking Algorithm Based on RIS Selection

Considering that richer spatial information can be provided for beam tracking when multiple RISs are assisted in communication, the study in this paper focuses on the development of a joint beam tracking system based on RIS selection. The previous subsection describes the design of a quantitative metric in RIS selection that depends on the location of the vehicle and the RIS. Since different numbers of RISs at different locations will have an impact on the beam tracking performance, the goal of this paper is to select as few RISs as possible as well as to select RISs at appropriate locations to assist the beam tracking.

Specifically, tracking is aided by having as few RISs as possible so that the system quantitative metrics can be greater than the predefined performance threshold τ_{th}. This maximizes beam tracking performance while reducing complexity and cost, achieving a balance between performance and resource efficiency. Next, the RIS selection strategy is described in detail, using $\mathcal{I}=3$ as an example. First of all, determine the benchmark of beam tracking performance, namely $\overline{\gamma}=\gamma_{\mathrm{R1}}^{(\kappa|\kappa-1)}+\gamma_{\mathrm{R2}}^{(\kappa|\kappa-1)}+\gamma_{\mathrm{R3}}^{(\kappa|\kappa-1)}$. Secondly, the resulting $\gamma_{\mathrm{R}|i|}^{(\kappa|\kappa-1)}$ is sorted in decreasing order as $\gamma_{\mathrm{R1}}^{(\kappa|\kappa-1)}\geq\gamma_{\mathrm{R2}}^{(\kappa|\kappa-1)}\geq\gamma_{\mathrm{R3}}^{(\kappa|\kappa-1)}$. If $\gamma_{\mathrm{R1}}^{(\kappa|\kappa-1)}/\overline{\gamma}\geq\tau_{\mathrm{th}}$, then 1 RIS is selected for auxiliary communication, where the set of selected RISs is $\mathcal{R}=\{\mathrm{R1}\}$. If $\gamma_{\mathrm{R1}}^{(\kappa|\kappa-1)}/\overline{\gamma}<\tau_{\mathrm{th}}$ and $(\gamma_{\mathrm{R1}}^{(\kappa|\kappa-1)}+\gamma_{\mathrm{R2}}^{(\kappa|\kappa-1)})/\overline{\gamma}\geq\tau_{\mathrm{th}}$, then 2 RISs are selected to aid communication, where the set of selected RISs is $\mathcal{R}=\{\mathrm{R1},\mathrm{R2}\}$. If none of the previously selected RISs can meet the performance threshold, all three RISs deployed in the scenario must participate in the auxiliary communication, and the set of selected RISs is $\mathcal{R}=\{\mathrm{R1},\mathrm{R2},\mathrm{R3}\}$. When more than one RIS has been selected to assist in the communication through the RIS selection strategy, the joint beam tracking algorithm used is shown in Eq. (63) through (66). This paper's complete joint beam tracking algorithm based on RIS selection is shown in Table 1. The computational complexity of the algorithm can be obtained as $O(N_n)$ based on the number of iterations.

3.4. Simulation Results and Analysis

In this section, the beam tracking system with the introduction of multi-RIS assistance is simulated and analyzed. The beam tracking performance is evaluated and compared for different cases by using Root Mean Squared Error (RMSE) $\mathrm{M}_x=\sqrt{\frac{1}{T}\sum_{\kappa=1}^{T}\left|x^{(\kappa)}-\hat{x}^{(\kappa)}\right|^2}$ and $\mathrm{M}_y=\sqrt{\frac{1}{T}\sum_{\kappa=1}^{T}\left|y^{(\kappa)}-\hat{y}^{(\kappa)}\right|^2}$, where T is the number of time slots. Consider the system with a bandwidth of $B=20\,\mathrm{MHz}$ and a center frequency of $f_c=28\,\mathrm{GHz}$. From this, the noise power magnitude is calculated as $\sigma_n^2=-174+10\lg(20\times10^6)\simeq-101\,\mathrm{dBm}$. The default number of antennas at the receiver and transmitter is 16; the path loss index is $n=2$; the time slot period size is $T_s=10\,\mathrm{ms}$; and the RSU height is set to $h_{\mathrm{RSU}}=10\,\mathrm{m}$. The initial speed of the vehicle is $v_0=10\,\mathrm{m/s}$; the deflection angle

TABLE 1. Joint beam tracking algorithm based on RIS selection.

Algorithm 1:Joint beam tracking algorithm based on RIS selection

Initialize:

1:Initialize state vector,$\boldsymbol{\mu}^{(0)}=\left[x^{(0)},y^{(0)},v^{(0)}\right]^{\mathrm{T}}$.

2:Initialize covariance matrix,$\mathbf{P}^{(0|0)}=\mathbf{0}_{3\times3}$.

Forecasting process

3:Status forecast update

$\hat{\boldsymbol{\mu}}^{(\kappa|\kappa-1)}=\mathbf{A}\hat{\boldsymbol{\mu}}^{(\kappa-1|\kappa-1)}$.

4:Compute the a priori covariance matrix.

$\mathbf{P}^{(\kappa|\kappa-1)}=\mathbf{A}\mathbf{P}^{(\kappa-1|\kappa-1)}\mathbf{A}^{\mathrm{T}}+\mathbf{Q}_\omega$

RIS Options:

5:In the deployed $\mathcal{I}$ RIS, the benchmark $\bar{\gamma}$ for beam tracking performance is determined based on the quantitative metrics of the design, and the performance threshold τ_{th} is defined

$\bar{\gamma}=\gamma_{\mathrm{R1}}^{(\kappa|\kappa-1)}+\gamma_{\mathrm{R2}}^{(\kappa|\kappa-1)}+\cdots+\gamma_{\mathrm{R}|\mathcal{I}|}^{(\kappa|\kappa-1)}$

6:Sort the resulting $\gamma_{\mathcal{I}}^{(\kappa|\kappa-1)}$ in descending order to obtain $\gamma_{\mathcal{I}}^{(\kappa|\kappa-1)}=\left[\gamma_{\mathrm{R1}}^{(\kappa|\kappa-1)},\gamma_{\mathrm{R2}}^{(\kappa|\kappa-1)},\cdots,\gamma_{\mathrm{R}|\mathcal{I}|}^{(\kappa|\kappa-1)}\right]$.

7:If $\gamma_{\mathcal{I}}^{(\kappa|\kappa-1)}(1)/\bar{\gamma}\geq\tau_{\mathrm{th}}$, then $I=1$, the chosen RIS is R1.

8:If $\gamma_{\mathcal{I}}^{(\kappa|\kappa-1)}(1)/\bar{\gamma}<\tau_{\mathrm{th}}$ and $\left(\gamma_{\mathcal{I}}^{(\kappa|\kappa-1)}(1)+\gamma_{\mathcal{I}}^{(\kappa|\kappa-1)}(2)\right)/\bar{\gamma}\geq\tau_{\mathrm{th}}$, then $I=2$, the chosen RIS is R1 and R2.

9:And so on, the RISs with good performance are selected for the joint auxiliary communication, and if none of the $\mathcal{I}-1$ RISs can satisfy the thresholds, then $I=\mathcal{I}$, all of the deployed $\mathcal{I}$ RISs are selected.

Correction process

10:Kalman gain matrix update

$$\mathbf{K}^{(\kappa)}=\mathbf{P}^{(\kappa|\kappa-1)}\left(\left(\boldsymbol{\rho}^{(\kappa)}\otimes\mathbf{I}_2\right)\tilde{\mathbf{G}}^{(\kappa|\kappa-1)}\right)^{\mathrm{T}}\left(\left(\boldsymbol{\rho}^{(\kappa)}\otimes\mathbf{I}_2\right)\tilde{\mathbf{G}}^{(\kappa|\kappa-1)}\mathbf{P}^{(\kappa|\kappa-1)}\left(\left(\boldsymbol{\rho}^{(\kappa)}\otimes\mathbf{I}_2\right)\tilde{\mathbf{G}}^{(\kappa|\kappa-1)}\right)^{\mathrm{T}}+\frac{\mathbf{I}_{2|I+1|}}{2}\right)^{-1}$$

11:Updating the a posteriori value of the system state estimate

$$\hat{\boldsymbol{\mu}}^{(\kappa|\kappa)}=\hat{\boldsymbol{\mu}}^{(\kappa|\kappa-1)}+\mathbf{K}^{(\kappa)}\left(\hat{\mathbf{s}}^{(\kappa)}-\left(\boldsymbol{\rho}^{(\kappa)}\otimes\mathbf{I}_2\right)\hat{\mathbf{h}}\left(\hat{\boldsymbol{\mu}}^{(\kappa|\kappa-1)}\right)\right)$$

12:Updating the a posteriori covariance matrix

$$\mathbf{P}^{(\kappa|\kappa)}=\left(\mathbf{I}_3-\mathbf{K}^{(\kappa)}\left(\boldsymbol{\rho}^{(\kappa)}\otimes\mathbf{I}_2\right)\tilde{\mathbf{G}}^{(\kappa|\kappa-1)}\right)\mathbf{P}^{(\kappa|\kappa-1)}$$

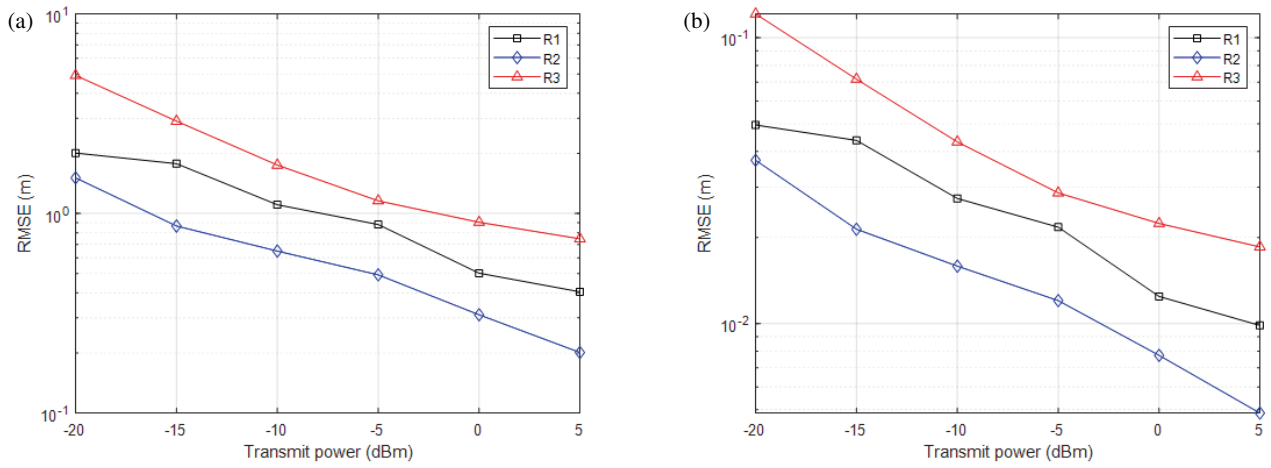

FIGURE 3. Comparison of beam tracking performance of single RIS with different deployment locations. (a) Tracking performance in x-coordinate. (b) Tracking performance in y-coordinate.

is $\pi/2^7$; and the duration of travel is 1 s. The number of RISs deployed in the scenario is $\mathcal{I} = 3$; the heights of all three RISs are set to $h_{\text{RIS}} = 10\,\text{m}$; the sizes of the UPAs are set to 4×4; and the coordinates are set to $(x_{\text{R1}}, y_{\text{R1}}) = (-20, 0)$, $(x_{\text{R2}}, y_{\text{R2}}) = (0, 10)$, and $(x_{\text{R3}}, y_{\text{R3}}) = (20, 0)$, respectively. Assume that the error parameter obeys a Gaussian distribution with standard deviation $\sigma_\omega = 10^{-0.5}$ and that the reference communication channel parameter is $\tilde{\beta} = 1$. The detailed system simulation parameters are shown in Table 2.

Figure 3 compares the impact of single RIS on beam tracking performance due to location deployment differences in the scenarios in this paper. At this time, the initial position of the vehicle is $(x_0, y_0) = (-15, 3)$. From Figure 3, it can be seen that R2 has better tracking than R1, and R3 is the worst. This is because R2 is closer to the RSU than R1 in the deployment position; the channel gain between R2 and the RSU is greater; and the vehicle is constantly moving closer to R2 and away from R1. From Eq. (16), the shorter the distance of the path is, the larger the average SNR of the antenna is. R1 tracks better than R3, because R1 is closer to the vehicle and has less path loss. Therefore, the distance of the RIS from the RSU and the vehicle affects the performance of beam tracking. Since the position of the RIS and RSU is fixed, the dynamic changes in the distance between the RIS and the vehicle should be taken into account when beam tracking is performed. So, it is necessary to use it as a measure of beam tracking performance when making RIS selection, as analyzed for Eq. (67). From Figure 3, it can also be seen that as the transmit power increases, the RMSE of both the x-coordinate and y-coordinate of a single RIS gradually decreases, and the RMSE of the y-coordinate is smaller than the RMSE of the x-coordinate. This is because in the established coordinate system, the main direction of travel of the vehicle coincides with the x-axis direction, and the movement on the y-axis is due to the deflection of the vehicle's motion being taken into account, but this deflection is at a smaller angle, which leads to a smaller tracking error in the y-coordinate than in the x-coordinate.

TABLE 2. System simulation parameters.

Simulation parameters	Retrieve value
Carrier frequency f_c	28 GHz
Bandwidth B	20 MHz
Noise power σ_n^2	-101 dBm
Number of transmitter antennas N_{T}	16
Number of receiving end antennas N_{R}	16
Path loss index n	2
Timeslot period T_s	10 ms
Vehicle initial speed v_0	10 m/s
Vehicle deflection angle φ	$\pi/2^7$
RSU height h_{RSU}	10 m
Total number of RIS deployed $\mathcal{I}$	3
RIS height h_{RIS}	10 m
Number of RIS array elements $N_{\text{RIS}} = N_{\text{x}} \times N_{\text{y}}$	4×4
RIS 1 coordinates $(x_{\text{R1}}, y_{\text{R1}})$	$(-20, 0)$
RIS 2 coordinates $(x_{\text{R2}}, y_{\text{R2}})$	$(0, 10)$
RIS 3 coordinates $(x_{\text{R3}}, y_{\text{R3}})$	$(20, 0)$
Error parameter σ_ω	$10^{-0.5}$
Power gain factor $\tilde{\beta}$	1

Figure 4 verifies the effect of the presence or absence of LoS paths and the number of RISs on the beam tracking performance of the BS-UE. The initial position coordinates of the vehicle are $(x_0, y_0) = (-30, 6)$, where "0L1R" indicates a scenario that there is no LoS path, and 1 RIS exists; "0L2R" indicates that there is no LoS path, and there are 2 RIS scenarios; "0L3R" indicates a scenario with no LoS path and the presence of 3 RIS; "1L1R" indicates the presence of LoS paths and 1 RIS scenario; "1L2R" indicates the presence of LoS paths and 2 RIS scenarios; "1L3R" indicates the presence of LoS paths and 3 RIS scenarios. From Figure 4, it can be seen that the RMSE in both x- and y-coordinates decreases as the transmit power increases. The RMSE for the y-coordinate is also lower than the RMSE for the x-coordinate, for the same detailed reasons as analyzed in Figure 3. For the same transmit power, as the number of RISs in the system increases, the RMSE in both x- and y-coordinate decreases, e.g., add another RIS to the "0L1R" scenario to make

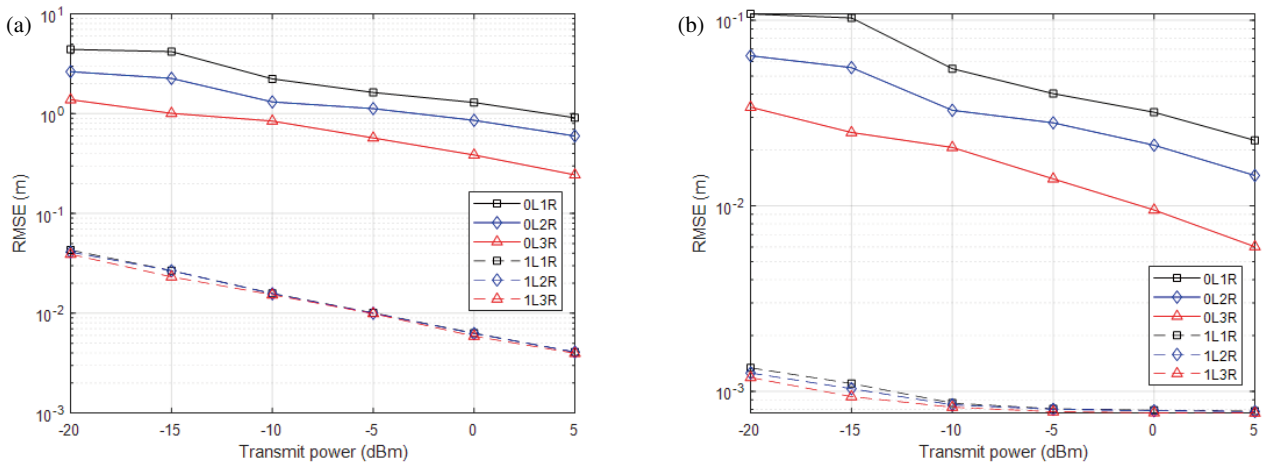

FIGURE 4. Comparison of beam tracking performance with different number of RISs. (a) Tracking performance in x-coordinate. (b) Tracking performance in y-coordinate.

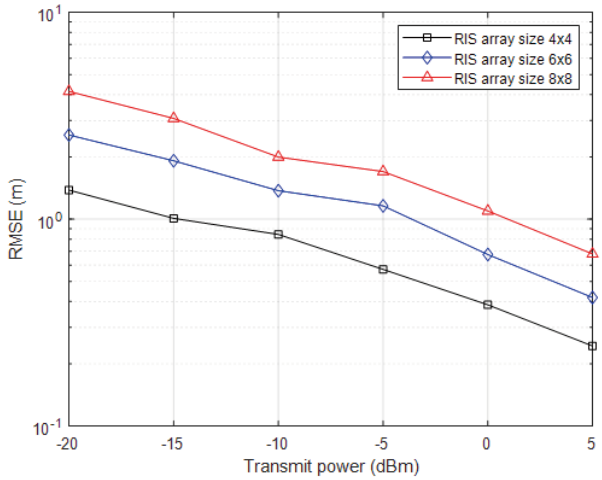

FIGURE 5. Tracking performance in x-coordinate.

it "0L2R" scenario, and the RMSE in the "0L2R" scenario is smaller than that in the "0L1R" scenario. Similarly, the RMSE decreases with the addition of the LoS path. Compared to the VLoS path constructed by RIS, the performance of beam tracking through the LoS path is better. Increasing the number of RISs in the presence of LoS paths has little effect on the improvement of beam tracking performance. This is because the transmission distance of the LoS path is smaller than that of the VLoS path; there is no reflection path; and the average SNR in the LoS path is larger than that of the VLoS path from Eq. (16). Therefore, the signal transmission quality is higher in direct-connected channels than cascaded channels. Overall, for RIS-assisted V2I communication systems, the beam tracking performance of the system can be improved by adding paths, either LoS paths or VLoS paths. Subsequently, for simulation simplicity and to focus on the core problem, only the x-coordinate, which has a larger tracking error and represents the main motion direction of the vehicle, is selected as the simulation object, and the existence of the LoS path is not considered.

Figure 5 compares the effect of different RIS array sizes on the beam tracking performance in the multi-RIS case. The initial position coordinates of the vehicle are $(x_0, y_0) = (-30, 6)$, $I = 3$, that is, three RISs are used to assist communication at the same time. From Figure 5, it can be seen that under the condition of the same transmit power, the tracking error is the largest when the RIS array size is 8×8, and the tracking error is the smallest when the RIS array size is 4×4. This indicates that although the multipath transmission environment created with the assistance of multiple RISs can provide more information such as beam angle and channel gain for beam tracking, at the same time increasing the number of units in the RIS does not improve the performance of beam tracking. This is because when the number of RIS units is increased, the beam width becomes narrower, and the narrower the beam is, the more sensitive it is to angular variations, and the beam will be more easily misaligned due to the presence of Gaussian process noise. Therefore, the tracking error due to beam misalignment cannot be fully compensated even in the case of multiple RIS. However, the RIS units should not be too few, as too few RIS units can result in a beam that is not sensitive enough to changes in Gaussian process noise. In practice, a balance can be struck between RIS array size and application effectiveness.

Before evaluating the performance of joint multi-RIS beam tracking, a single RIS at a suitable location is selected based on the RIS selection algorithm to assist beam tracking in order to verify the feasibility and advantages of the metrics proposed in this paper. Figure 6 studies the case of switching to the VLoS path constructed by a single RIS for communication when the LoS path is blocked, and the beam tracking performance is simulated and compared under the three approaches of using a fixed deployment of a single RIS, selecting a single RIS based on the SNR, and selecting a single RIS based on the metrics proposed in this paper, in which the vehicle's initial position coordinates are $(x_0, y_0) = (-20, 3)$. From Figure 8(a), it can be seen that R2 assisted tracking is better than R1. This is because the vehicle is approaching R2 from the initial position, and as the distance gets closer, the average SNR increases as shown in Eq. (16). On the other hand, the vehicle is moving away from R1 and getting farther away; the average SNR decreases; and the tracking performance decreases. From Fig-

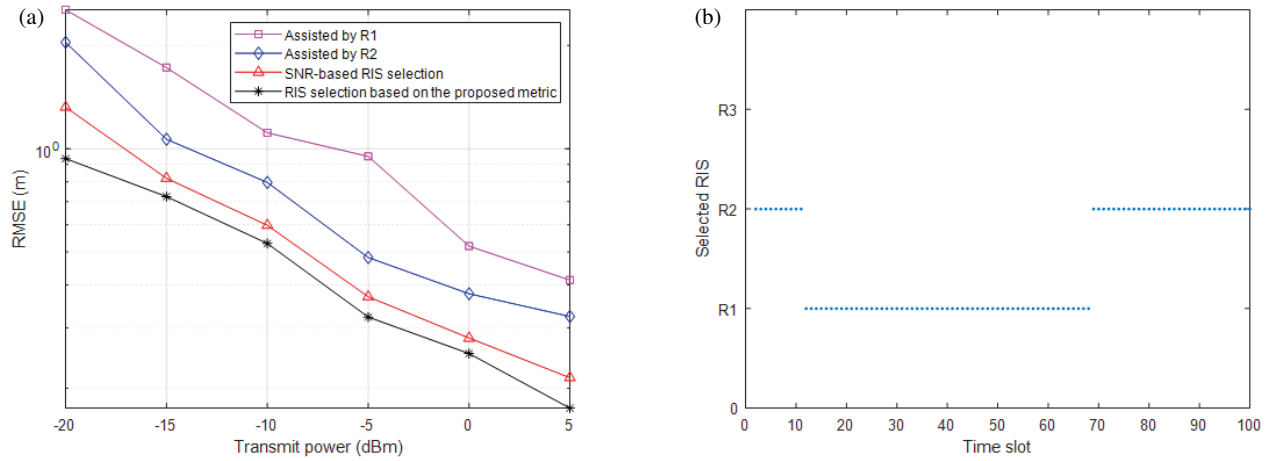

FIGURE 6. Comparison of beam tracking performance with single RIS selection under different metrics. (a) Impact of single RIS selection on tracking performance. (b) The process of adaptive single RIS selection.

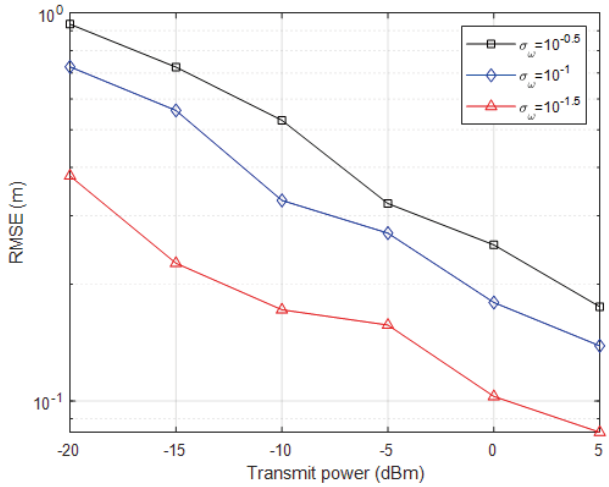

FIGURE 7. Tracking performance in x-coordinate.

ure 8(a), it can be seen that performing RIS selection is better than the fixed deployment of single RIS assistance. Through RIS selection, the RIS with the best performance can be chosen in each time slot, thereby compensating for the error accumulation caused by the EKF algorithm. The best tracking performance after RIS selection using the metrics proposed in this paper is because SNR, which contains the entire channel information, and the distance variation due to vehicle motion and beam angle variation are jointly used to evaluate the beam tracking performance, with comprehensive consideration of the factors. Figure 8(b) shows the RIS situation where the transmission power is -20 dBm, and the vehicle adaptively switches using the indicators proposed in this paper within 1 second, that is, 100 time slots. With the comparison of the simulation results in Figure 8(a), the feasibility and effectiveness of the indicators proposed in this paper are verified.

Figure 7 compares the effect of different speed error parameters on the beam tracking performance when a single RIS is selected based on the metrics proposed in this paper, where the standard deviation of the error parameter is set to $\sigma_\omega = \{10^{-1.5}, 10^{-1}, 10^{-0.5}\}$, and the vehicle's initial position coordinates are $(x_0, y_0) = (-20, 3)$. From Figure 7, it can be seen that the smaller the standard deviation of the error parameter is, the smaller the RMSE in x-coordinate is, i.e., the better the beam tracking performance is. This is because the speed error parameter is hypothetical noise that represents the amount of change in vehicle speed, and its magnitude reflects the distance traveled per unit of time. For the same deflection angle, the larger the velocity error parameter is, the larger the velocity component is in the x-axis direction, and the larger the tracking error is. Similarly, the smaller the velocity error parameter is, the smaller the velocity component is in the x-axis direction, and the smaller the tracking error is. In IoV systems, the faster the speed is, the more likely the beam will be out of alignment, then the worse the tracking will be.

Figure 8 compares the tracking performance of the joint beam tracking algorithms performed with different metrics, where the initial position coordinate of the vehicle is $(x_0, y_0) = (10, 5)$, and the duration of traveling is 1.5 s. When joint beam tracking is performed based on SNR, the threshold is set to $\tau_{\text{th}} = 0.65$. The threshold is set to $\tau_{\text{th}} = 0.95$ for joint beam tracking based on the proposed metrics. Setting different thresholds for different metrics is to ensure that the value of I is at most 2 during RIS selection, that is, three RISs will not be selected at the same time to assist communication. From Figure 8(a), it can be seen that the joint beam tracking system based on the proposed metrics has better performance than the system based on single RIS selection, which is because the direction change of the reflected beams from multiple RISs is jointly considered in the tracking process, which provides more information for beam tracking. This is consistent with the conclusion in Figure 4 that the higher the number of RISs is involved in the assist, the better the beam tracking performance of the system is. However, RISs in different positions have different tracking performances. The number of RISs cannot be considered only, and the assisting effect of RIS in the same number of different positions is a big difference, as shown in the simulation Figure 3. The performance of the system after joint beam tracking by the proposed metrics is compared with the performance of the system in which the three RISs deployed in the scene are

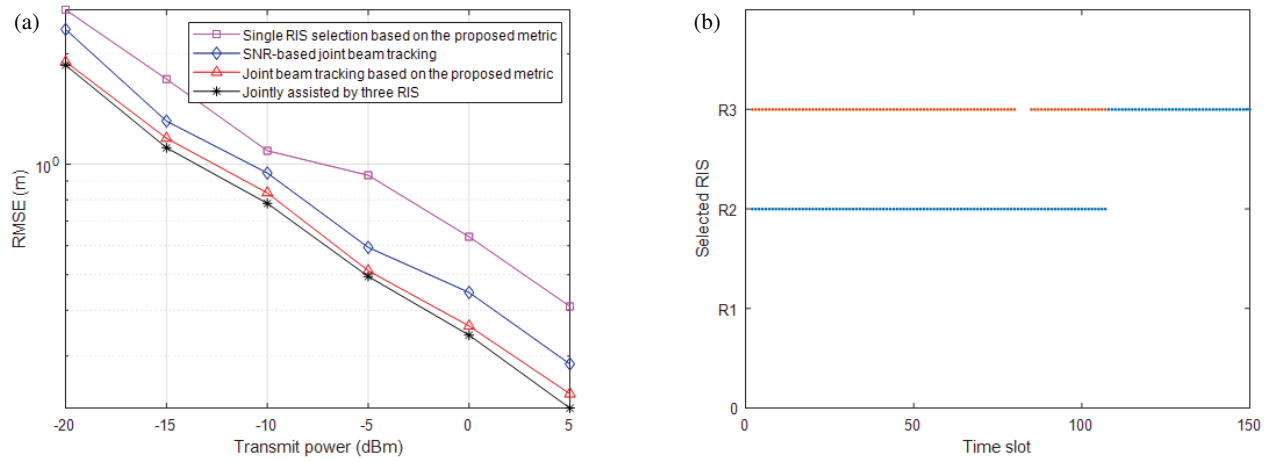

FIGURE 8. Performance comparison of joint beam tracking algorithms with different metrics. (a) Effect of multiple RIS selection on tracking performance. (b) The process of adaptive RIS selection.

simultaneously involved in the assistance. It can be seen from Figure 8(a) that the gap between the two is smaller in general, because the RIS deployed in a distant location has a larger path loss, and the vehicle is far away from this RIS in the process of traveling, so it has a small assisting effect. Meanwhile, the joint beam tracking system based on the proposed metric has lower tracking error than the SNR-based joint beam tracking system. Figure 8(b) shows the RIS situation where the transmission power is 5 dBm, and the vehicle makes RIS selection using the proposed indicators within 1.5 seconds, that is, 150 time slots. It is observed that at most 2 RISs are selected simultaneously during the RIS selection process, and there are cases where 1 RIS is selected in some time slots, and the overall beam tracking performance has a small gap compared to the full process using 3 RISs. As a result, the joint beam tracking algorithm based on the proposed metrics can maximize the performance of beam tracking as well as resource utilization while choosing as few RISs as possible to aid in communication. Above simulation experiments verify that the joint beam tracking algorithm with the proposed metrics in this paper is more advantageous than the SNR-based beam tracking algorithm.

4. CONCLUSION

In millimeter-wave MIMO systems, a joint beam tracking algorithm based on RIS selection is proposed in this paper, considering the three-dimensional scenario of multi-RIS deployment. Based on the state model of position and speed, the V2I beam tracking model under the combined path is derived, and the beam tracking is realized based on the EKF algorithm. Distinguishing from traditional RIS selection metrics, the performance of RIS-assisted V2I beam tracking was quantified in terms of received SNR, beam angle variation, and RIS-to-vehicle distance variation. Based on this quantitative metric, an EKF joint beam tracking algorithm based on RIS selection is designed. The beam tracking performance for different cases is simulated and analyzed using RMSE as the performance metric. Simulation results show that the joint beam tracking algorithm with the proposed metrics in this paper performs better than the conventional SNR-based beam tracking algorithm. Subsequently, in order to improve the performance of beam tracking, the communication model of V2V can be introduced. More useful information can be provided for beam tracking through V2V and V2I collaborative transmission.

ACKNOWLEDGEMENT

This work was supported by the Natural Science Foundation of Fujian Province (Grant No. 2022J011276, and No. 2023I0044), Undergraduate Education and Teaching Research Project of Fujian Province (Grant No. FBJY20240120), High-level Talent Project of Xiamen University of Technology (Grant No. YKJ22030R, and No. YKJ23034R), and Postgraduate Science and Technology Innovation Project of Xiamen University of Technology (Grant No. YKJCX2024143).

REFERENCES

[1] Chen, S., Y. Shi, and J. Hu, "Cellular vehicle to everything (C-V2X): A review," *Bulletin of National Natural Science Foundation of China*, Vol. 34, No. 2, 179–185, 2020.

[2] Zhang, L., Y. Wang, J. Tian, L. Zhang, and T. Zhang, "Joint beam forming design for IRS-aided MIMO Internet of vehicles system," *Journal on Communication/Tongxin Xuebao*, Vol. 44, No. 2, 59, 2023.

[3] Noor-A-Rahim, M., Z. Liu, H. Lee, M. O. Khyam, J. He, D. Pesch, K. Moessner, W. Saad, and H. V. Poor, "6G for vehicle-to-everything (V2X) communications: Enabling technologies, challenges, and opportunities," *Proceedings of the IEEE*, Vol. 110, No. 6, 712–734, 2022.

[4] Yu, D., G. Zheng, A. Shojaeifard, S. Lambotharan, and Y. Liu, "Kalman filter based channel tracking for RIS-assisted multi-user networks," *IEEE Transactions on Wireless Communications*, Vol. 23, No. 4, 3856–3869, 2024.

[5] Jung, J.-S., C.-Y. Park, J.-H. Oh, and H.-K. Song, "Intelligent reflecting surface for spectral efficiency maximization in the multi-user MISO communication systems," *IEEE Access*, Vol. 9, 134 695–134 702, 2021.

[6] Meng, X., F. Liu, C. Masouros, W. Yuan, Q. Zhang, and Z. Feng, "Vehicular connectivity on complex trajectories: Roadway-geometry aware ISAC beam-tracking," *IEEE Transactions on*

Wireless Communications, Vol. 22, No. 11, 7408–7423, 2023.

[7] Yu, X., L. Tu, Q. Yang, M. Yu, Z. Xiao, and Y. Zhu, "Hybrid beamforming in mmWave massive MIMO for IoV with dual-functional radar communication," *IEEE Transactions on Vehicular Technology*, Vol. 72, No. 7, 9017–9030, 2023.

[8] Saqib, N. U., S. Hou, S. H. Chae, and S.-W. Jeon, "Reconfigurable intelligent surface aided hybrid beamforming: Optimal placement and beamforming design," *IEEE Transactions on Wireless Communications*, Vol. 23, No. 9, 12 003–12 019, 2024.

[9] Zhang, P., J. Zhang, H. Xiao, H. Du, D. Niyato, and B. Ai, "RIS-aided 6G communication system with accurate traceable user mobility," *IEEE Transactions on Vehicular Technology*, Vol. 72, No. 2, 2718–2722, 2023.

[10] Barb, G. and M. Otesteanu, "4G/5G: A comparative study and overview on what to expect from 5G," in *2020 43rd International Conference on Telecommunications and Signal Processing (TSP)*, 37–40, Milan, Italy, 2020.

[11] Yao, J., W. Xu, Y. Huang, H. Xiao, and Z. Lu, "Techniques for reconfigurable intelligent surfaceaided 6G communication network: An overview," *Journal of Signal Processing*, Vol. 38, No. 8, 1555–1567, 2022.

[12] Wu, Q., S. Zhang, B. Zheng, C. You, and R. Zhang, "Intelligent reflecting surface-aided wireless communications: A tutorial," *IEEE Transactions on Communications*, Vol. 69, No. 5, 3313–3351, 2021.

[13] Chen, W., X. Lin, J. Lee, A. Toskala, S. Sun, C. F. Chiasserini, and L. Liu, "5G-advanced toward 6G: Past, present, and future," *IEEE Journal on Selected Areas in Communications*, Vol. 41, No. 6, 1592–1619, 2023.

[14] Teng, B., X. Yuan, R. Wang, and S. Jin, "Bayesian user localization and tracking for reconfigurable intelligent surface aided MIMO systems," *IEEE Journal of Selected Topics in Signal Processing*, Vol. 16, No. 5, 1040–1054, 2022.

[15] Chen, Y., D. Yue, J. Ren, S. Bai, and a. Y. Sun, "Research on performance of multi-reconfigurable intelligent surface assisted communication system," *Radio Engineering*, Vol. 52, 2124–2131, 2022.

[16] Pan, C., G. Zhou, K. Zhi, S. Hong, T. Wu, Y. Pan, H. Ren, M. D. Renzo, A. L. Swindlehurst, R. Zhang, and A. Y. Zhang, "An overview of signal processing techniques for RIS/IRS-aided wireless systems," *IEEE Journal of Selected Topics in Signal Processing*, Vol. 16, No. 5, 883–917, 2022.

[17] Wei, Y., M.-M. Zhao, A. Liu, and M.-J. Zhao, "Channel tracking and prediction for IRS-aided wireless communications," *IEEE Transactions on Wireless Communications*, Vol. 22, No. 1, 563–579, 2023.

[18] Yildirim, I., A. Uyrus, and E. Basar, "Modeling and analysis of reconfigurable intelligent surfaces for indoor and outdoor applications in future wireless networks," *IEEE Transactions on Communications*, Vol. 69, No. 2, 1290–1301, 2021.

[19] Ning, B., P. Wang, L. Li, Z. Chen, and J. Fang, "Multi-IRS-aided multi-user MIMO in mmWave/THz communications: A space-orthogonal scheme," *IEEE Transactions on Communications*, Vol. 70, No. 12, 8138–8152, 2022.

[20] Li, M., Y. Cao, J. Yan, and J. Lu, "Method on millimeter wave cascade channel estimation assisted by multiple intelligent reflecting surface," *Journal of Beijing University of Posts and Telecommunications*, Vol. 46, No. 4, 15–20, 2023.

[21] Mirza, J., B. Ali, and M. A. Javed, "Stable matching for selection of intelligent reflecting surfaces in multiuser MISO systems," *IEEE Communications Letters*, Vol. 25, No. 8, 2748–2752, 2021.

[22] Yang, L., Y. Yang, D. B. d. Costa, and I. Trigui, "Outage probability and capacity scaling law of multiple RIS-aided networks," *IEEE Wireless Communications Letters*, Vol. 10, No. 2, 256–260, 2021.

[23] Fang, Y., S. Atapattu, H. Inaltekin, and J. Evans, "Optimum reconfigurable intelligent surface selection for wireless networks," *IEEE Transactions on Communications*, Vol. 70, No. 9, 6241–6258, 2022.

[24] Mensi, N. and D. B. Rawat, "Reconfigurable intelligent surface selection for wireless vehicular communications," *IEEE Wireless Communications Letters*, Vol. 11, No. 8, 1743–1747, 2022.

[25] Song, J., S.-H. Hyun, J.-H. Lee, J. Choi, and S.-C. Kim, "Joint vehicle tracking and RSU selection for V2I communications with extended Kalman filter," *IEEE Transactions on Vehicular Technology*, Vol. 71, No. 5, 5609–5614, 2022.

[26] Hyun, S.-H., J. Song, K. Kim, J.-H. Lee, and S.-C. Kim, "Adaptive beam design for V2I communications using vehicle tracking with extended Kalman filter," *IEEE Transactions on Vehicular Technology*, Vol. 71, No. 1, 489–502, 2022.

[27] Song, J., J.-H. Lee, and S. Noh, "Position-based adaptive beamforming and roadside unit sectorization for V2I communications," *IEEE Transactions on Vehicular Technology*, Vol. 73, No. 2, 2960–2965, 2024.

[28] El Ayach, O., S. Rajagopal, S. Abu-Surra, Z. Pi, and R. W. Heath, "Spatially sparse precoding in millimeter wave MIMO systems," *IEEE Transactions on Wireless Communications*, Vol. 13, No. 3, 1499–1513, 2014.

[29] Liu, F., W. Yuan, C. Masouros, and J. Yuan, "Radar-assisted predictive beamforming for vehicular links: Communication served by sensing," *IEEE Transactions on Wireless Communications*, Vol. 19, No. 11, 7704–7719, 2020.

[30] Shaham, S., M. Ding, M. Kokshoorn, Z. Lin, S. Dang, and R. Abbas, "Fast channel estimation and beam tracking for millimeter wave vehicular communications," *IEEE Access*, Vol. 7, 141 104–141 118, 2019.